ラー制度[6](表1)を実施している．制度の有無や申し込み方法（原則的に医師からの依頼申し込みが一般的）は地方自治体の保健福祉部などや感染症対策の関連部局に問い合わせるとよい．

院内で入院中に告知を受ける場合には，受検者は感染告知後に自分の病状や治療について誰かに聞きたい，また今後のことに不安を感じてだれかに相談したいと思ったときに院内のスタッフをつかまえることが可能である．しかし，医療機関の外来や保健所などの検査所で告知を受けた場合，次回の診察や紹介されたHIV診療病院を受診するまでの期間は周囲からの支援において最も脆弱な期間といえるだろう．この期間の支援のリソースとして，**HIV感染者を対象とする電話相談がエイズ予防財団や各地域のNGOやNPOの支援団体によって実施されている**[7]ので，それらを紹介することを勧めたい．

おわりに

医療機関での診療や治療が始まった後にも，HIV感染者はHIV感染症とともに生きることから生じるさまざまな心理・社会的な課題を抱える可能性がある．たとえば，仕事などの社会生活と治療の両立，パートナーや家族など周囲の人への病名告知，いままでもっていた家族関係の問題の顕在化，将来への不安，ライフサイクル上（結婚，出産，子育てなど）の課題，性指向を巡る葛藤などである[8]．これらについては，**医療職と心理・社会的援助専門職（臨床心理士，心理職，社会福祉士，精神保健福祉士など）による継続的な支援**が必要である．

(参考文献)

1) HIV検査・相談マップ(http://www.hivkensa.com/index.html)
2) 花澤佳子，浦尾充子，金井明美，石川雅子，池上　宏：保健所におけるHIV抗体検査受検者に対するカウンセリングの意義について―抗体検査に伴う不安の検討から―．日本エイズ学会誌，3(3)：136-139, 2001.
3) エイズ予防財団：エイズ電話相談 0120-177-812(祝祭日を除く月～金曜日 10：00～13：00, 14：00～17：00)
4) 山中京子：若年者とHIV感染―性行動の現状と予防介入の課題―．東京医学社，周産期医学，32(2)：159-162, 2002.
5) 山中京子：感染告知後のカウンセリング，HIV Q&A．岡　慎一(編)，医薬ジャーナル社，42-44, 2002.
6) 全国で派遣カウンセリング制度を実施している地方自治体については，実施地方自治体のリストを参照．
7) エイズ予防情報ネット(API-Net：NGO一欄参照(http://api-net.jfap.or.jp/htmls/frameset-09.html)
8) 野島一彦，矢永由里子：HIVと心理臨床―最前線からの報告―心理臨床の実践と課題．ナカニシヤ出版，京都，2002.

THE JOURNAL OF BIOLOGICAL CHEMISTRY VOL. 281, NO. 2, pp. 1241–1250, January 13, 2006
Printed in the U.S.A.

Altered HIV-1 Gag Protein Interactions with Cyclophilin A (CypA) on the Acquisition of H219Q and H219P Substitutions in the CypA Binding Loop*

Received for publication, May 31, 2005, and in revised form, November 7, 2005 Published, JBC Papers in Press, November 7, 2005, DOI 10.1074/jbc.M505920200

Hiroyuki Gatanaga[‡1], Debananda Das[‡], Yasuhiro Suzuki[‡§], Damaris D. Yeh[‡], Khaja A. Hussain[¶], Arun K. Ghosh[¶], and Hiroaki Mitsuya[‡§2]

From the [‡]Experimental Retrovirology Section, HIV and AIDS Malignancy Branch, NCI, National Institutes of Health, Bethesda, Maryland 20892, the [§]Departments of Hematology and Infectious Diseases, Kumamoto University School of Medicine, Kumamoto 860, Japan, and the [¶]Department of Chemistry, University of Illinois, Chicago, Illinois 60607

HIV-1 Gag protein interaction with cyclophilin A (CypA) is critical for viral fitness. Among the amino acid substitutions identified in Gag noncleavage sites in HIV-1 variants resistant to protease inhibitors, H219Q (Gatanaga, H., Suzuki, Y., Tsang, H., Yoshimura, K., Kavlick, M. F., Nagashima, K., Gorelick, R. J., Mardy, S., Tang, C., Summers, M. F., and Mitsuya, H. (2002) *J. Biol. Chem.* 277, 5952–5961) and H219P substitutions in the viral CypA binding loop confer the greatest replication advantage to HIV-1. These substitutions represent polymorphic amino acid residues. We found that the replication advantage conferred by these substitutions was far greater in CypA-rich MT-2 and H9 cells than in Jurkat cells and peripheral blood mononuclear cells (PBM), both of which contained less CypA. High intracellular CypA content in H9 and MT-2 cells, resulting in excessive CypA levels in virions, limited wild-type HIV-1 (HIV-1_{WT}) replication and H219Q introduction into HIV-1 (HIV-1_{H219Q}), reduced CypA incorporation of HIV-1, and potentiated viral replication. H219Q introduction also restored the otherwise compromised replication of HIV-1_{P222A} in PBM, although the CypA content in HIV-$1_{H219Q/P222A}$ was comparable with that in HIV-1_{P222A}, suggesting that H219Q affected the conformation of the CypA-binding motif, rendering HIV-1 replicative in a low CypA environment. Structural modeling analyses revealed that although hydrogen bonds are lost with H219Q and H219P substitutions, no significant distortion of the CypA binding loop of Gag occurred. The loop conformation of HIV-1_{P222A} was found highly distorted, although H219Q introduction to HIV-1_{P222A} restored the conformation of the loop close to that of HIV-1_{WT}. The present data suggested that the effect of CypA on HIV-1 replicative ability is bimodal (both high and low CypA content limits HIV-1 replication), that the conformation of the CypA binding region of Gag is important for viral fitness, and that the function of CypA is to maintain the conformation.

Combination antiretroviral therapy has brought about improved quality of life and extended survival in patients with HIV-1[3] infection. However, the emergence of HIV-1 variants resistant to anti-HIV-1 therapeutic agents, including reverse transcriptase inhibitors and protease inhibitors (PIs), has limited the efficacy of chemotherapy (1). HIV-1 develops resistance mainly by substituting amino acids in the target viral enzyme or component; however, recent studies have revealed that certain polymorphic amino acid residues also contribute to the viral resistance (2, 3). We recently found that multiple amino acid substitutions emerged in noncleavage sites of the Gag protein, which were associated with the development of HIV-1 resistance against PIs (4). Among such amino acid substitutions, H219Q, occurring in the cyclophilin A (CypA) binding loop in the p24 Gag protein, conferred the greatest replication advantage on HIV-1 (4). CypA binds to p24 Gag protein, resulting in the packaging of ~200 copies of CypA into each HIV-1 virion (5, 6), and is thought to perform an essential role early in the HIV-1 replication cycle (7, 8), perhaps by destabilizing the capsid (p24 Gag protein) shell during viral entry and uncoating (9) and/or by performing an additional chaperon function, facilitating correct capsid condensation during viral maturation (10, 11).

In the present study, we asked how H219Q and H219P substitutions occurring within the viral CypA binding loop conferred replication advantage to HIV-1, and we examined whether these substitutions affected the conformation and interaction of p24 Gag protein and CypA during HIV-1 propagation in various host cells. We also attempted to better understand the functional role of CypA in HIV-1 replication. To that end, we determined the virological and biochemical properties of a variety of recombinant infectious clones and their CypA contents. We also carried out molecular modeling analyses of the wild-type and mutated p24 Gag complex with CypA. The data demonstrate that both H219Q and H219P enhance HIV-1 replication by reducing viral CypA contents in daughter virions as produced in CypA-rich cells, but not in cells that has a low CypA content. We suggest that the effect of CypA on HIV-1 replicative ability is bimodal, both high and low contents of CypA limit HIV-1 replication. The data also suggest that the conformation of p24 Gag is strongly correlated with viral fitness.

EXPERIMENTAL PROCEDURES

Antiviral Agents—Three PIs, KNI-272, JE-2147, and UIC-94003, were synthesized as described previously (12–16). Three newly synthesized PIs, UIC-00041, UIC-00142, and UIC-00145 (Fig. 1), were also

* This work was supported in part by the Intramural Research Program of the NCI, Center for Cancer Research, National Institutes of Health, in part by National Institutes of Health Grant GM 53386 (to A. K. G.), in part by Research for the Future Program Grant JSPS-RFTF 97L00705 from the Japan Society for the Promotion of Science (to H. M.), a grant-in-aid for scientific research (priority areas) from the Ministry of Education (to H. M.), a grant from the Culture, Sports, Sciences, and Technology of Japan (Monbu-Kagakusho) (to H. M.), and a grant for the promotion of AIDS research from the Ministry of Health Welfare and Labor of Japan (Kosei-Rohdosho) (to H. M.). The costs of publication of this article were defrayed in part by the payment of page charges. This article must therefore be hereby marked "*advertisement*" in accordance with 18 U.S.C. Section 1734 solely to indicate this fact.

[1] Present address: AIDS Clinical Center, International Medical Center of Japan, Tokyo 162-8655, Japan.

[2] To whom correspondence should be addressed: Experimental Retrovirology Section, HIV and AIDS Malignancy Branch, NCI, National Institutes of Health, Bldg. 10, Rm. 5A11, 9000 Rockville Pike, Bethesda, MD 20892. Tel.: 301-496-9238; Fax: 301-402-0709; E-mail: hmitsuya@helix.nih.gov.

[3] The abbreviations used are: HIV-1, human immunodeficiency virus, type 1; PBM, peripheral blood mononuclear cell; CHRA, competitive HIV-1 replication assay; CypA, cyclophilin A; PI, protease inhibitor; PHA, phytohemagglutinin; CsA, cyclosporin A; CA, capsid; WT, wild type.

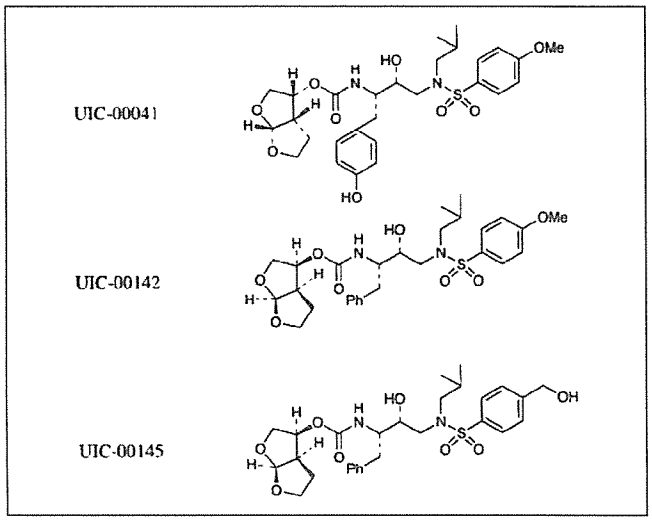

FIGURE 1. **Structures of UIC-00041, UIC-00142, and UIC-00145.**

synthesized by Ghosh and Hussain,[4] and the procedures for the synthesis will be published elsewhere.

Generation of HIV-1 Variants Resistant to PIs—The wild-type infectious clone, HIV-1_{WT}, produced by COS-7 cells transfected with pHIV-1_{NL4-3} was propagated in human $CD4^+$ MT-2 or H9 cells in the presence of increasing concentrations of an antiretroviral agent as described previously (4, 14, 16). Briefly, MT-2 or H9 cells (5×10^5) were exposed to wild-type HIV-1_{NL4-3} and cultured in the presence of each PI at initial concentrations of 0.0005–0.03 μM. When the virus began to propagate in the presence of the drug, the drug concentration was increased. This selection was carried out for a total of 27–80 passages. For the generation of JE-2147-resistant virus, an infectious clone carrying I84V substitution in the protease (HIV-1_{I84V}) was employed instead of HIV-1_{WT} (14). Proviral DNA in the lysates of HIV-1-infected cells of the last passage was sequenced as indicated (4).

Generation of Recombinant HIV-1 Clones—To generate HIV-1 clones carrying the desired mutations, the site-directed mutagenesis was performed, and the mutation-containing genomic fragments thus obtained were introduced to pHIV-1_{NLSma} as described previously (4). An infectious clone containing P222A mutation in Gag was generated using a plasmid kindly provided by Drs. D. Braaten and J. Luban (5). Each recombinant plasmid was transfected into COS-7 cells, and the obtained infectious virions were harvested 48 h after transfection and stored at −80 °C until use (4).

Replication Kinetic Assay—MT-2, H9, Jurkat cells (10^5), or phytohemagglutinin-stimulated peripheral blood mononuclear cells (PHA-PBM: 5×10^6) were exposed to each infectious virus preparation (500 blue-cell-forming units defined in the MAGI assay) (17) for 12 h, washed twice with phosphate-buffered saline, and cultured in 5 ml of complete medium in the presence or absence of cyclosporin A (CsA). Culture supernatants (200 μl) were harvested every other day or every 4 days, and p24 Gag amounts were determined using a commercially available radioimmunoassay kit (PerkinElmer Life Sciences). An enzyme-linked immunosorbent assay kit (Beckman Instruments, Fullerton, CA) was also used for the determination of p24 Gag amounts as needed.

Competitive HIV-1 Replication Assay Using PHA-PBM—In order to compare the replication rates of infectious HIV-1 clones, the competitive HIV-1 replication assay (CHRA) was performed as described previously (18) with some modifications. In brief, PHA-PBMs (5×10^6) were exposed to various mixtures of the paired infectious clones to be examined for their replicative ability and were cultured for the indicated times. Every 7 days, the supernatants of the virus co-culture were transferred to freshly prepared uninfected PHA-PBM cultures. DNA purified from the cells harvested at each passage was subjected to direct DNA sequencing of the HIV-1 genome, and viral population changes were evaluated based on relative peak heights in the electropherogram (18).

Western Blot Analysis—For the analysis of cellular CypA contents, MT-2 cells, H9 cells, Jurkat cells, or PHA-PBMs were lysed with lysis buffer (4), and the amounts of lysates were normalized with cell numbers or total protein contents using a bicinchoninic acid protein assay kit (Pierce). For the analysis of virion-associated CypA, the culture supernatants of chronically HIV-1-infected H9 or Jurkat cells were centrifuged and passed through a 0.22-μm pore-size filter to remove cellular debris; the filtrates were normalized with p24 contents measured with radioimmunoassay and were ultracentrifuged to pellet virions (4). The pelleted virions were lysed in lysis buffer. The resultant samples were processed with SDS-polyacrylamide gradient gels, and CypA was visualized by SuperSignalWestPico (Pierce) using anti-CypA antiserum (Biomol, Plymouth Meeting, PA). An anti-p24 Gag antiserum (Advanced Biotechnologies, Inc., Columbia, MD) served as a control to ensure that appropriate amounts of the samples were loaded. The signal density of CypA and p24 Gag was analyzed on a Windows computer by using the ImageJ Program (developed at National Institutes of Health, rsb.info.nih.gov/ij/) as published previously (19).

Molecular Modeling of the $p24_{CA151}$-CypA Complex with p24 Amino Acid Substitutions—The crystal structure of human CypA that was bound to the amino-terminal domain of p24 Gag (capsid residues 1–151 (CA_{151}), Protein Data Bank code 1AK4) (9) was analyzed to determine the changes with H219Q or H219P substitution. There were two CA-CypA complexes in the structure. Chain A of CypA and chain D of CA form one complex and were retained for the calculation. Identical results should be obtained with the other complex (chain B of CypA and chain C of CA) because the conformations of both CypA and CA in these complexes are quite similar. Structural modifications, visualization, and analysis were performed utilizing the Maestro interface from Schrödinger (Maestro 7.0, Schrödinger, LLC, New York). OPLS2003 force field (20) as implemented in MacroModel 9.0 (MacroModel, version 9.0, Schrödinger, LLC, New York) was used for minimizing mutated structures and for carrying out molecular dynamics calculations. OPLS2003 uses an enhanced version of the widely used OPLS-AA force field and has improved parameters for peptides. It was verified that the force field had high quality bond stretching, bending, and torsional parameters. Charges were taken from the force field. Molecular dynamics calculations were carried out on the wild-type complex and on the mutated structures. The structures were initially minimized for 2500 iterations. A constant temperature of 300 K and SHAKE constraints for bonds to hydrogens were used. The GB/SA continuum solvation model, with water as the solvent, was used (21). While calculating nonbonded interactions, cut-off distances of 8 and 20 Å were used for van der Waals and electrostatic interactions, respectively. Using a time step of 2 fs, the structures were equilibrated for 20 ps, and the simulation was carried out for 1 ns. Structures were monitored at intervals of every 50 ps. Calculations were carried out on an SGI Origin 3400 computer platform. For the wild type and for each mutant structure, 1-ns molecular dynamics calculation takes about 11 days under the stated conditions on this high performance computational platform.

[4] A. K. Ghosh and K. A. Hussain, personal communication.

TABLE 1

Amino acid substitutions identified in the protease and p24 Gag protein of HIV-1 variants selected against PI

Amino acid substitutions listed are based on the amino acid sequences deduced from the nucleotide sequence of the protease-encoding and the entire Gag-encoding genes of each HIV-1 selected against an indicated PI.

PI	Strain	Cell	Passage	Amino acid substitutions identified in	
				Protease	p24
KNI-272	HIV-1_{NL4-3}[a]	MT-2	27	V32I/M46I/V82I/I84V	H219Q
KNI-272	HIV-1_{LAI}	H9	55	V32I/L33F/K45I/F53L/A71V/I84V	H219Q
APV	HIV-1_{NL4-3}[a]	MT-2	31	L10F/V32I/M46I/I54M/A71V/I84V	H219Q
JE-2147	HIV-$1_{NL4-3/I84V}$[a]	MT-2	33	M46I/I47V/V82I/I84V	H219Q
UIC-94003	HIV-1_{NL4-3}[a]	MT-2	62	L10F/A28S/M46I/I50V/A71V	Q199H/H219Q
UIC-00041	HIV-1_{NL4-3}	MT-2	73	K43I/L63P/V82I	M200I/H219P
UIC-00142	HIV-1_{NL4-3}	MT-2	84	L10F/V32I/M46I/I84V	H219Q
UIC-00145	HIV-1_{NL4-3}	MT-2	80	L10F/V32I/M46I/I47A/K55N	H219Q

[a] PI-resistant HIV-1 variants described previously (4) are shown.

RESULTS

Amino Acid Substitutions Identified in p24 Gag Protein in HIV-1 Variants Resistant to PI—We have reported previously that several amino acid substitutions were seen in common in the Gag protein at noncleavage sites among HIV-1 variants that acquired *in vitro* a high multitude of resistance to PIs such as APV, JE-2147, KNI-272, and UIC-94003 (4). In an attempt to corroborate and extend our previous observations and to determine how often such amino acid substitutions develop in the Gag protein, we examined four more HIV-1 variants that were selected *in vitro* against various PIs, including three novel PIs, UIC-00041, UIC-00142, and UIC-00145. Table 1 depicts the properties of eight PI-resistant HIV-1 variants (including four HIV-1 variants reported previously). Seven of the eight variants were selected against PIs in MT-2 cells, although one variant was selected in H9 cells. The strains used were HIV-1_{NL4-3} and HIV-1_{LAI}, and 3–6-amino acid substitutions were identified in the protease. It was noted that all eight variants had in common an amino acid substitution at position 219 in p24 Gag protein, seven variants had H219Q substitution and one had H219P substitution. The His^{219} residue is located within the CypA binding loop and is thought to play a role in the p24 Gag interactions with CypA through a hydrogen bond and hydrophobic contact(s) (9). It is worth noting that when HIV-1_{NL4-3} was propagated in the absence of PI in MT-2 cells, the virus also acquired H219Q, V218M, or A224V mutation by passage 10 (4). It should be noted that two amino acids, Val^{218} and Ala^{224}, are also located within the CypA binding loop of the p24 Gag protein and are also known to interact with CypA through hydrophobic contacts (9). These data, taken together, strongly suggest that the amino acids interacting with CypA, in particular His^{219}, are prone to undergo substitutions under certain circumstances and are associated with viral replication fitness. Indeed, in the HIV Sequence Compendium 2000 (22), of 88 different HIV-1 strains, 65 had histidine at the position 219, whereas 13 had glutamine, and 4 had proline at the position 219, indicating that both Gln^{219} and Pro^{219} represent polymorphic amino acid residues. Hence, the present data suggest that these two polymorphic amino acids are associated with viral fitness and possibly to the acquisition of resistance to certain PIs.

Effects of Gag Mutations at Position 219 on HIV-1 Replication—In order to examine the effects of the Gag mutation at position 219 on HIV-1 replication, we generated two infectious HIV-1 clones, HIV-1_{H219Q} and HIV-1_{H219P}, and we assessed their virologic properties. In MT-2 cells, HIV-1_{H219Q} rapidly replicated compared with the wild-type HIV-$1_{WT(His-219)}$ (Fig. 2*A*), in agreement with our previous observation (4). HIV-1_{H219Q} also replicated more rapidly than HIV-1_{WT} in H9 cells (Fig. 2*B*). HIV-1_{H219P} replicated as rapidly as HIV-1_{H219Q}, suggesting that the amino acid at position 219 is critical for the replication fitness of HIV-1. When we examined the fitness of the three infectious clones (HIV-1_{WT}, HIV-1_{H219Q}, and HIV-1_{H219P}) in $CD4^+$ Jurkat cells and PHA-PBM, there was no significant difference seen in their replication fitness (Fig. 2, *C* and *D*).

Competitive HIV-1 Replication Assays for H219Q Mutation in PHA-PBM—As shown above, although HIV-1_{H219Q} exhibited a greater replication capability when propagated in MT-2 and H9 cells compared with HIV-1_{WT}, there was no apparent difference in the replication profiles of HIV-1_{H219Q} and HIV-1_{WT} as propagated in PHA-PBM (Fig. 2, *A*, *B* and *D*). In order to evaluate the possible biological relevance of the replication kinetic data generated by using immortalized and long term cultured MT-2 and H9 cells, we conducted a modified competitive HIV-1 replication assay (CHRA) (18), in which freshly prepared PHA-PBM served as host cells. HIV-1_{H219Q} readily and uniformly overgrew HIV-1_{WT} in CHRA regardless of three different ratios of paired clones used in the assay (Fig. 2, *E–G*). These data indicated that the H219Q substitution conferred replication advantages on HIV-1 when propagated in immortalized $CD4^+$ T cells as well as PHA-PBM. It should be noted, however, that the replication advantage of HIV-1 acquired with the H219Q substitution was limited in PHA-PBM and was detected only when assessed with CHRA.

MT-2 and H9 Cells Contain Greater Amounts of CypA—The Gag mutations H219Q and H219P conferred significant replication advantage on HIV-1 as propagated in MT-2 cells and H9 cells, but such advantage was limited in PHA-PBM. Considering that His^{219} is located within the CypA binding loop and that HIV-1 replication is known to be affected by intracellular CypA contents (6, 7), we examined intracellular CypA content in each cell preparation by using Western blot analysis. As shown in Fig. 3, *A* and *B*, the CypA contents in 10^4 MT-2 (relative density, 100%) and 10^4 H9 cells (79.6%) appeared to be greater than those in 5×10^4 Jurkat cells (55.4%) and 5×10^4 PHA-PBM (42.9%), suggesting that MT-2 and H9 cells contained 6–12 times as much CypA per cell as Jurkat cells and PHA-PBM. As normalized with total cellular protein amounts, the CypA content in 1 μg of MT-2 and H9 cellular protein preparations was comparable with that in 2–4 μg of Jurkat protein preparations and that in 4 μg of PHA-PBM protein, suggesting that the former two cell preparations contained 2–4-fold greater amounts of CypA per cellular protein than the latter two cell preparations. These data showed that MT-2 and H9 cells have greater CypA amounts than Jurkat T cells and PHA-PBM.

Decreased CypA Incorporation into HIV-1_{H219Q} Virions—Considering that the data from crystal structure analyses by Gamble *et al.* (9) of p24 Gag protein complexed with CypA showing that His^{219} binds to Asn^{71} and Gln^{111} of CypA through a hydrogen bond and hydrophobic contact(s), respectively, we postulated that H219Q and H219P substitutions cancel or weaken such hydrogen bonds, resulting in the reduction of p24 binding to CypA and of CypA incorporation into daughter virions, leading to increased HIV-1 replication in CypA-rich MT-2 and H9 cells. We then examined the virion-associated CypA amounts in

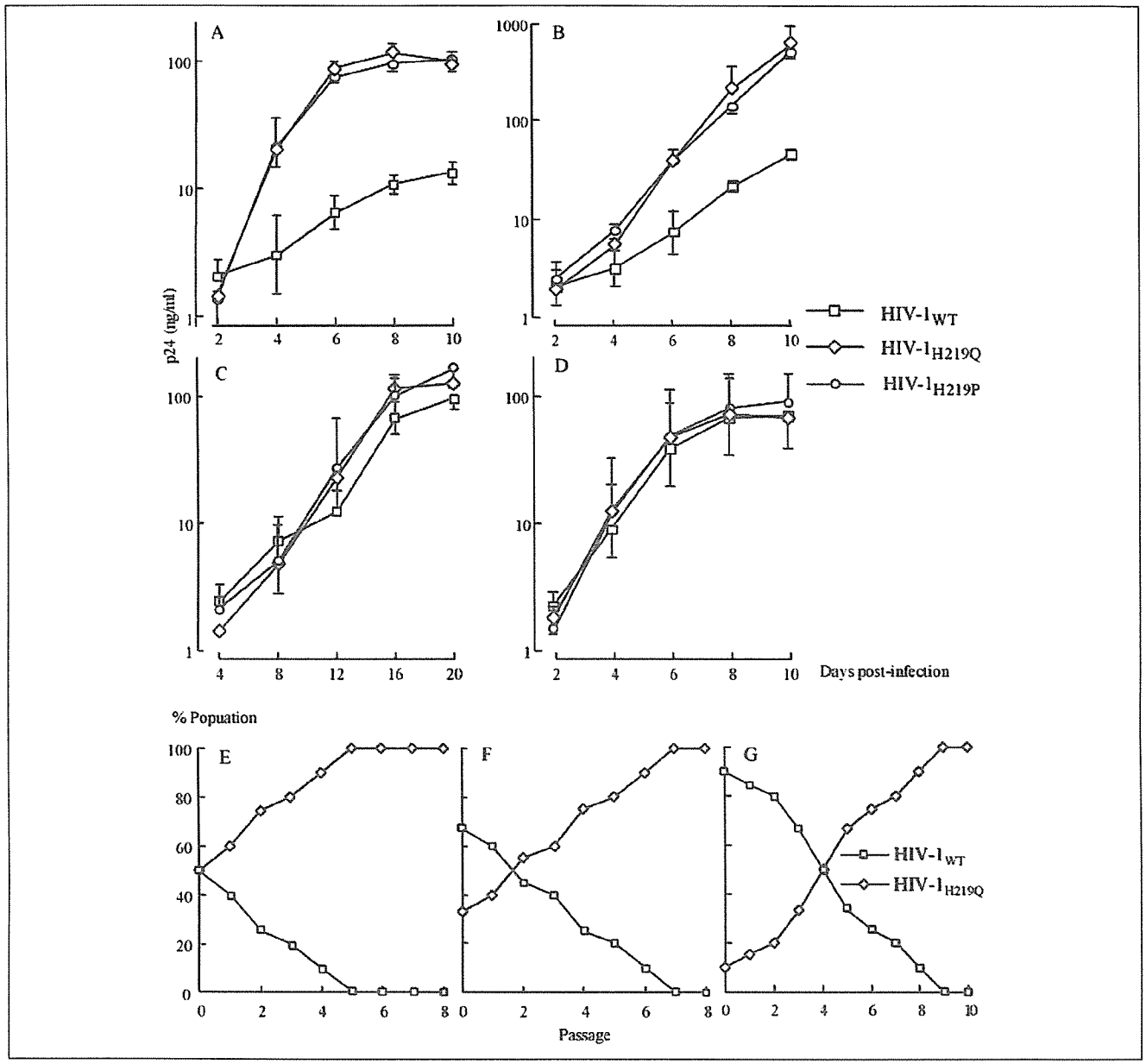

FIGURE 2. **Replication kinetics of HIV-1_{WT}, HIV-1_{H219Q}, and HIV-1_{H219P}.** MT-2 cells, H9 cells, Jurkat cells, and PHA-PBM (*A–D*, respectively) were exposed to each HIV-1 clone and cultured for the indicated numbers of passage. Virus replication was monitored by measuring the amounts of p24 Gag protein produced in the culture supernatants. The data shown represent geometric means (± 1 S.D.) of three independent experiments. Replication profiles of HIV-1_{WT} and HIV-1_{H219Q} in PHA-PBM were examined using CHRA (*E–G*). Two infectious HIV-1 clones to be compared for their fitness were mixed and propagated in PHA-PBM. The cell-free supernatant was transferred to fresh PHA-PBM every 7 days. The ratios of HIV-1_{WT} and HIV-1_{H219Q} at the initiation of the assay were 50:50, 67:33, and 90:10 (*E–G*, respectively). High molecular weight DNA extracted from infected cells at the end of each passage was subjected to nucleotide sequencing, and the proportions of His and Gln at position 219 in Gag protein were determined.

three infectious HIV-1 clones containing HIV-1_{WT}, HIV-1_{H219Q}, and HIV-1_{H219P}, employing Western blotting analysis using anti-p24 Gag and anti-CypA antisera. The culture supernatants of chronically HIV-1-infected H9 cells were prepared to contain the same amount of p24. The virions in each supernatant thus prepared were pelleted by ultracentrifugation and subsequently subjected to SDS-PAGE. Direct sequencing of cellular DNA confirmed that no unintended mutations developed during the culture. As shown in Fig. 3*C-1–3*, the experiment was performed three times. Percent densities of the CypA signal relative to each p24 Gag signal (making each signal 100%) were 11.1, 7.38, and 6.01% (Fig. 3*C-1*); 6.99, 4.99, and 4.71% (Fig. 3*C-2*), and 18.1, 12.0, and 11.2% (Fig. 3*C-3*) for HIV-1_{WT}/H9, HIV-1_{H219Q}/H9, and HIV-1_{H219P}/H9, respectively. These data demonstrated that H219Q and H219P substitutions increased HIV-1 replication in CypA-rich cells, which was associated with the substantial reduction of CypA incorporation into daughter virions.

p24 Gag Binding to CypA Affects HIV-1 Replication Kinetics—Yin *et al.* (23) have reported that the addition of CsA (0.5 μM) reduces CypA incorporation into daughter virions and increases replication rates of HIV-1_{1NL4-3} in H9 cells, suggesting that excessively high intracellular CypA contents may reduce HIV-1 replication rates. We then examined the effects of CsA on the replication rates of HIV-1_{WT} (Fig. 4, *A–D*) and HIV-1_{H219Q} (Fig. 4, *E–H*) in four different cell preparations.

In MT-2 and H9 cells, 0.5 μM CsA increased the replication rate of HIV-1_{WT}, whereas at a higher concentration (2.5 μM) its replication rate

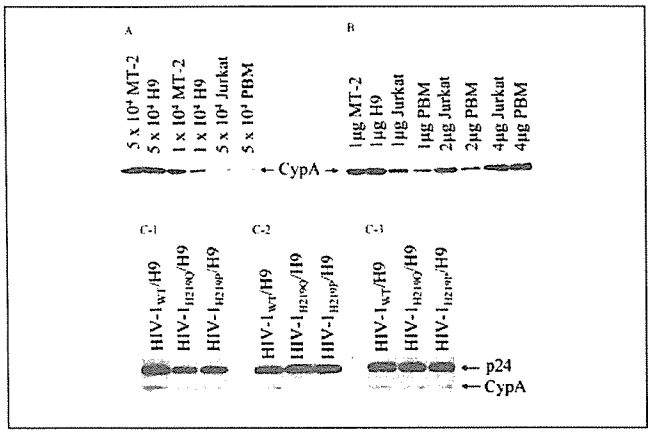

FIGURE 3. **MT-2 and H9 cells contain greater amounts of CypA than Jurkat cells and PHA-PBM, and HIV-1_{H219Q} and HIV-1_{H219P} virions contain reduced amounts of CypA than HIV-1_{WT} virions.** MT-2 cells, H9 cells, Jurkat cells, and PHA-PBM were lysed with lysis buffer, and the samples loaded were normalized by cell numbers or total protein contents. CypA was visualized with Western blotting analysis using anti-CypA antiserum (*A* and *B*). Percent CypA signal densities in 5×10^4 MT-2 cells, 5×10^4 H9 cells, 1×10^4 H9 cells, 5×10^4 Jurkat cells, and 5×10^4 PHA-PBM were 340.1, 387.4, 79.6, 55.4, and 42.9%, respectively, as compared with that in 1×10^4 MT-2 cells (serving as a standard to be 100%) (*A*). Percent CypA signal densities in 1 μg of H9 cells, 1 μg of Jurkat cells, 1 μg of PBM, 2 μg of Jurkat cells, 2 μg of PBMs, 4 μg of Jurkat cells, and 4 μg of PBMs were 155.2, 70.6, 35.0, 131.1, 59.5, 258.3, and 126.0%, respectively, as compared with that in 1 μg of MT-2 cells (serving as a standard to be 100%) (*B*). HIV-1 virions in the culture supernatants of chronically HIV-1-infected H9 cells were pelleted and subjected to Western blotting analysis for the determination of virion-associated CypA amounts using anti-p24 Gag and anti-CypA antisera. This experiment was performed three times (*C-1–3*). Percent densities of the CypA signal relative to each p24 Gag signal (making each p24 signal 100%) were 11.1, 7.38, and 6.01% in *C-1*; 6.99, 4.99, and 4.71% in *C-2*; and 18.1, 12.0, and 11.2% in *C-3* for HIV-1_{WT}/H9, HIV-1_{H219Q}/H9, and HIV-1_{H219P}/H9, respectively.

was reduced (Fig. 4, *A* and *B*), in agreement with the data by Yin *et al.* (23). In contrast, in Jurkat cells no increase in replication rate was seen, but rather CsA decreased HIV-1_{WT} replication in a dose-dependent manner (Fig. 4*C*). In PHA-PBM, CsA significantly decreased the replication rate of HIV-1_{WT}, and with 2.5 and 10 μM CsA, HIV-1_{WT} only poorly replicated (Fig. 4*D*). These data suggest that CsA (0.5 μM) can potentiate HIV-1_{WT} replication only in CypA-rich host cells. We further examined the effects of CsA on the replication of HIV-1_{H219Q} under the same conditions. In MT-2 and H9 cells (Fig. 4, *E* and *F*), no replication enhancement was seen with CsA added, but rather a reduced replication rate was observed in the presence of 0.5, 2.5, and 10 μM CsA. In Jurkat cells and PHA-PBM, the addition of CsA reduced the replication rate of HIV-1_{H219Q} as seen with HIV-1_{WT} (Fig. 4, *G* and *H*).

Taken together, the data suggest that the high intracellular CypA content in MT-2 and H9 cells was prohibitive to the replication of HIV-1_{WT} and that an appropriate concentration of CsA enhanced HIV-1_{WT} replication in CypA-rich cells by reduction of CypA incorporation into virions. In case of HIV-1_{H219Q}, however, H219Q already had reduced CypA incorporation into virions, and no enhanced replication was seen even in CypA-rich cells.

Effects of H219Q and P222A Substitutions on HIV-1 Replication—An amino acid substitution at position 222 from Pro to Ala (P222A) has been shown to substantially decrease the binding of p24 Gag protein to CypA and the CypA incorporation into daughter virions, causing reduced HIV-1 replication in Jurkat cells (6). As shown in Fig. 5, *A* and *B*, as examined in MT-2 and H9 cells, HIV-1_{NL4-3} carrying P222A (HIV-1_{P222A}) had a relatively low replication rate compared with HIV-1_{WT} in both host cells. However, with the introduction of both H219Q and P222A substitutions, HIV-$1_{H219Q/P222A}$ acquired faster replication rate; it replicated more rapidly than HIV-1_{WT} in MT-2 cells and comparably in H9 cells. In contrast, as examined in Jurkat cells, HIV-1_{P222A} showed a substantially decreased replication rate (Fig. 5*C*). In PHA-PBM, HIV-1_{P222A} was virtually replication-incompetent (Fig. 5*D*). As expected, with the H219Q substitution added, HIV-$1_{H219Q/P222A}$ exhibited an improved replication rate, which, however, yet remained below that of HIV-1_{WT} both in Jurkat cells and PHA-PBM (Fig. 5, *C* and *D*).

These data suggested either that the added H219Q substitution enabled HIV-1_{P222A} to incorporate more CypA into daughter virions or that H219Q altered or restored a conformation of the CypA binding domain of p24 Gag protein, thereby rendering the virus replication-competent without increasing CypA content.

H219Q Substitution Improves HIV-1_{P222A} Fitness without Increasing CypA Content—In order to ask whether H219Q improved the otherwise compromised CypA incorporation caused by the P222A substitution into virions or H219Q rendered HIV-1_{P222A} replication-competent without increasing CypA content, we examined the virion-associated CypA amounts by employing Western blotting analysis.

As can be seen in Fig. 5*E-1–3*, as HIV-1 virions in the culture supernatants of chronically HIV-1-infected H9 or Jurkat cells were pelleted and subjected to Western blotting analysis for the determination of virion-associated CypA amounts using anti-p24 Gag and anti-CypA antisera, the percent densities of the CypA signal relative to each p24 Gag signal (making each p24 signal 100%) were 33.8, 8.03, 6.92, and 6.48% in Fig. 5*E-1*; 26.3, 14.1, 6.93, and 6.19% in Fig. 5*E-2*; and 16.8, 6.48, 5.72, and 5.51% in Fig. 5*E-3* for HIV-1_{WT}/H9, HIV-1_{WT}/Jurkat, HIV-1_{P222A}/H9, and HIV-$1_{H219Q/P222A}$/H9, respectively, although HIV-$1_{H219Q/P222A}$ had a greater replication rate compared with HIV-1_{P222A} (Fig. 5, *A–E*).

These data demonstrated that HIV-1_{WT} produced by Jurkat cells and HIV-1_{P222A} produced by H9 cells contained approximately less than half and approximately one-fourth of the CypA amount detected in HIV-1_{WT} produced by H9 cells, respectively. The data strongly suggested that H219Q altered the conformation of the CypA binding domain of p24 Gag protein without affecting the CypA incorporation into HIV-1_{P222A} virions, thus rendering HIV-1_{P222A} replication relatively independent of CypA. It is possible that H219Q substitution not only decreased the incorporation of CypA into HIV-1 but also altered the conformation of Gag protein, thus leading to increased HIV-1 replication especially when HIV-1 is produced in CypA-rich cells. The latter effect of H219Q substitution is apparently viable in the presence of P222A substitution because increased HIV-$1_{H219Q/P222A}$ replication was seen without significant changes in CypA content in virions (Fig. 5, *A–E*).

Molecular Modeling of the p24 Gag CA_{151}-CypA Complex with H219Q or H219P—We finally carried out molecular modeling studies to better understand the following two aspects: the reason for less viral incorporation of CypA with H219Q, H219P, and P222A substitutions, and the rescue of viral replication with the H219Q/P222A double mutation. The crystal structure determined by Gamble *et al.* (9) revealed the sequence-specific interactions of p24 Gag (CA_{151}) with CypA (Fig. 6*A*). Those interactions include seven hydrogen bonds between residues 219 and 223 (excluding the bonds mediated through bridging water molecules) and various hydrophobic contacts, all of which appear to stabilize the interactions between p24 Gag and CypA (Fig. 6*B*). Our molecular dynamics calculations for 1 ns show valuable insights to the changes in interaction between wild-type and mutated p24 Gag and CypA. Initially, the change in conformation of the wild-type structure as well as the fluctuation of the hydrogen bonds between CA and CypA at intervals of 50 ps up to 1 ns was analyzed. The backbone conformation essentially remains the same even though there is loss of the hydrogen bonds between His^{219} and $Asn^{71}{}_{CypA}$ during this dynamics calculation. The

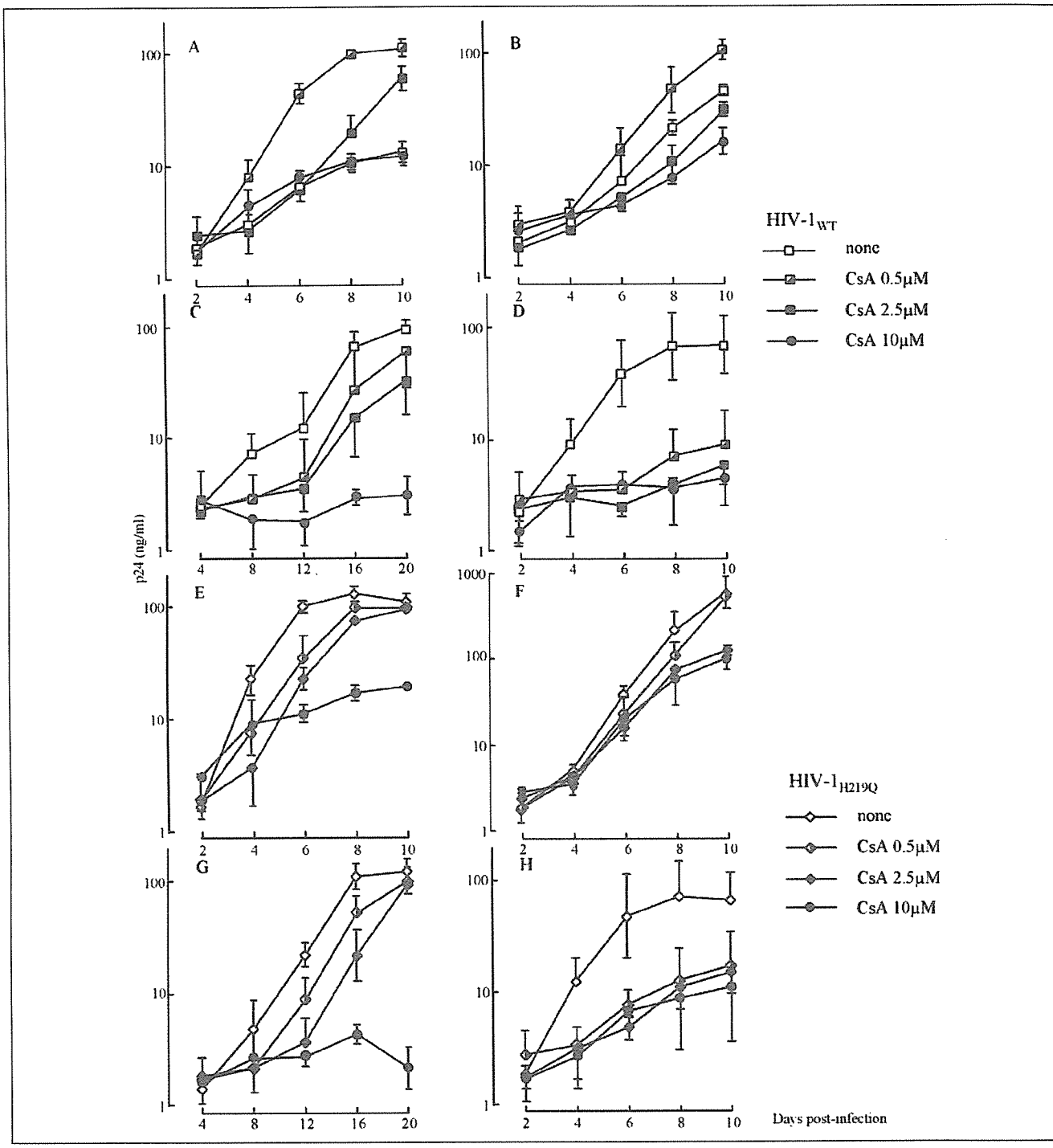

FIGURE 4. **Effects of CsA on HIV-1_{WT} and HIV-1_{H219Q} replication in various cell cultures.** MT-2 cells, H9 cells, Jurkat cells, and PHA-PBMs (*A–D*, respectively) were exposed to HIV-1_{WT} and cultured in the presence or absence of 0.5, 2.5, or 10 μM CsA. MT-2 cells, H9 cells, Jurkat cells, and PHA-PBMs (*E–H*, respectively) were also exposed to HIV-1_{H219Q} and cultured in the presence or absence of 0.5, 2.5, or 10 μM CsA. Virus replication was monitored with the amounts of p24 produced in the culture supernatants. The data shown represent geometric means (± 1 S.D.) of three independent experiments.

hydrogen bonds between Pro^{222} and $Arg^{55}{}_{CypA}$, Gly^{221}–$Asn^{102}{}_{CypA}$, and Ala^{220}–$Gln^{63}{}_{CypA}$ are the most invariant. Theses data suggest that the backbone conformation of the CypA binding region of p24 Gag is maintained with the mutation at position 219. For the mutated structures, the loop conformations at the end of 1 ns of molecular dynamics calculation were compared with the wild-type crystal structure. The weighted root mean square differences of the structures were calculated after a best fit of residues from Val^{218} to Ala^{224}. The root mean square differences of CA_{H219Q} from the wild-type CA_{151} was only 0.99 Å. Even though there is loss of hydrogen bond interactions with H219Q substitution, the loop conformations that depend on the overall conformational contact between CA and CypA do not undergo significant change (Fig. 6, *C* and *D*). The loss of the hydrogen bond between residue 219 of CA and CypA reduces the strong interaction between CA and CypA

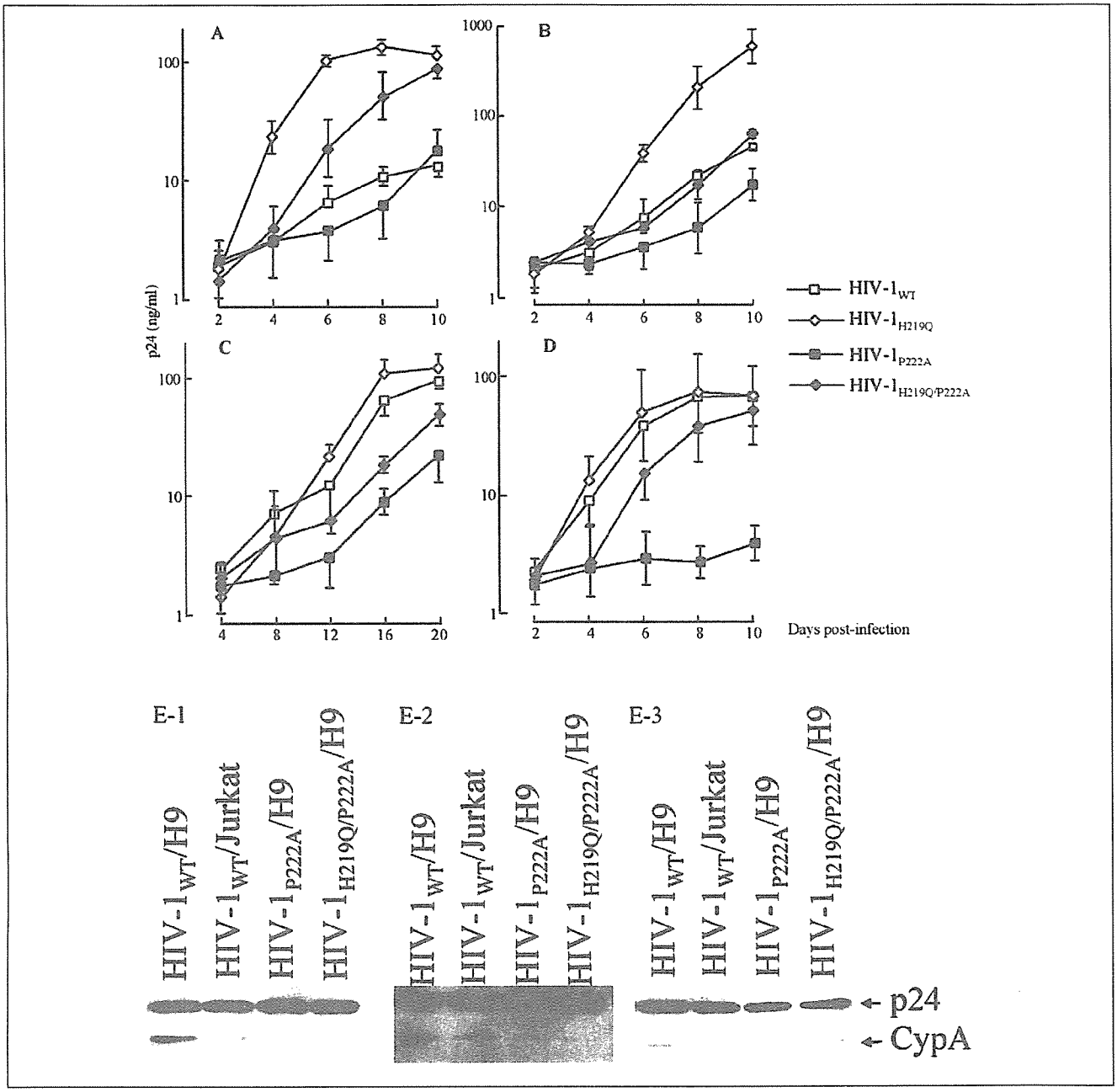

FIGURE 5. **Replication kinetics of HIV-1_{WT}, HIV-1_{H219Q}, HIV-1_{P222A}, and HIV-$1_{H219Q/P222A}$ and virion-associated CypA amounts in various HIV-1 preparations.** MT-2 cells, H9 cells, Jurkat cells, and PHA-PBMs (*A–D*, respectively) were exposed to each HIV-1 clone and cultured. Virus replication was monitored with the amount of p24 produced in the culture supernatants. The data shown represent geometric means (± 1 S.D.) of three independent experiments. HIV-1 virions in the culture supernatants of chronically HIV-1-infected H9 or Jurkat cells were pelleted and subjected to Western blotting analysis for the determination of virion-associated CypA amounts using anti-p24 Gag and anti-CypA antisera. This experiment was performed three times (*E-1–3*). Percent densities of the CypA signal relative to each p24 Gag signal (making each p24 signal 100%) were 33.8, 8.03, 6.92, and 6.48% in *E-1*; 26.3, 14.1, 6.93, and 6.19% in *E-2*; and 16.8, 6.48, 5.72, and 5.51% in *E-3* for HIV-1_{WT}/H9, HIV-1_{WT}/Jurkat, HIV-1_{P222A}/H9, and HIV-$1_{H219Q/P222A}$/H9, respectively.

and in a CypA-rich environment helps in improving viral replication. As shown in Fig. 7*A*, in the ribbon diagram of CA_{P222A} superimposed on that of CA_{WT}, CA_{P222A} causes a significant distortion of the loop structure. The value of weighted root mean square deviation of the structure of CA_{P222A} from CA_{WT} structure is 3.16 Å. In comparison, as can be seen in the ribbon diagrams of the structures of the CypA binding region of various mutant CA species (Fig. 7*B*), generated with 1-ns dynamics calculations and superimposed on the structure of CA_{WT}, H219Q and H219P substitutions do not significantly affect the conformation of the CypA binding region of CA_{WT}.

Effects of H219Q and P222A Substitutions on the Conformation of the CypA Binding Loop—It is of note that P222A not only results in less CypA incorporation but the significant change in loop conformation is probably responsible for reduction in viral replication. That the loop conformation is responsible for viral fitness is further evidenced by analysis of the structures with concurrent H219Q and P222A substitutions. These two concurrent substitutions recovered the distortion of the loop conformation that was associated with P222A mutation alone (Fig. 7*A*). Fig. 7*B* illustrates that the conformations of the CypA binding region of CA_{WT} and mutant CA species structurally resemble each other. The

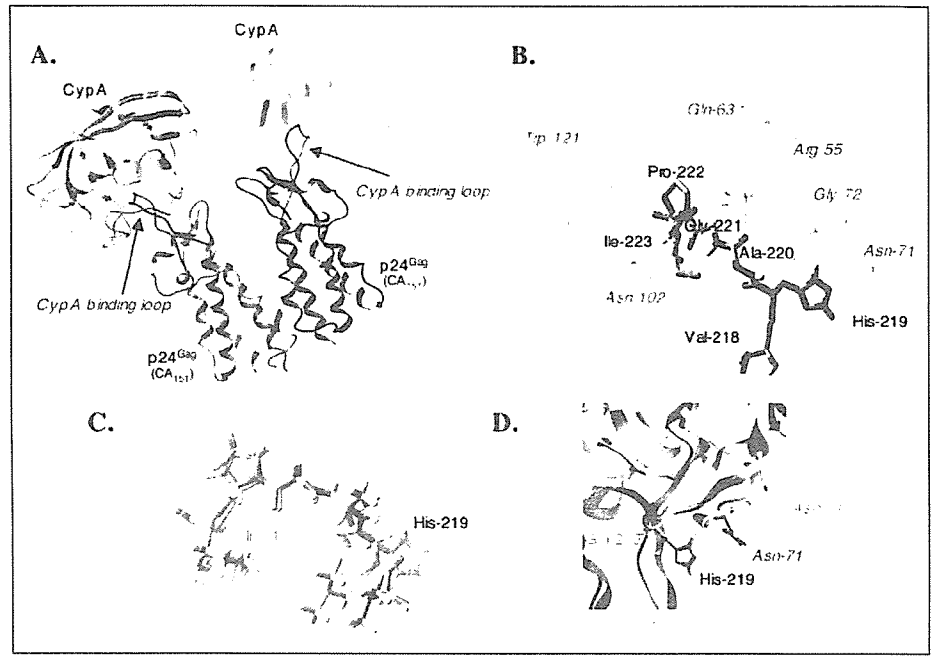

FIGURE 6. **Loss of hydrogen bonds in CA_{151}-CypA complex with H219Q or H219P substitution.** *A*, there are two p24 Gag CA_{151}-CypA complexes in the asymmetric unit (9). *B*, in the area of the CypA binding loop shown there are seven hydrogen bonds, which are between His^{219}–$Asn^{71}{}_{CypA}$, Ala^{220}–$Gln^{63}{}_{CypA}$, Ala^{220}–$Gly^{72}{}_{CypA}$, Gly^{221}–$Asn^{102}{}_{CypA}$, Pro^{222}–$Arg^{55}{}_{CypA}$ (two hydrogen bonds), and Ile^{223}–$Trp^{121}{}_{CypA}$. These hydrogen bonds along with hydrophobic contacts are responsible for maintaining the optimum relative conformations of p24 and CypA. *C*, H219Q substitution results in the loss of the following three hydrogen bond interactions: Gln^{219}–$Asn^{71}{}_{CypA}$, Ala^{220}–$Gly^{72}{}_{CypA}$, and Ile^{223}–$Trp^{121}{}_{CypA}$ and causes a significant conformational change of the contact region of the CypA binding loop (see *D*). *D*, changes in the complex configurations with H219Q substitution. Note that in the mutated structure Gln^{219} (*wire*) is located far apart from $Asn^{71}{}_{CypA}$ (*wire*), although in the wild-type structure His^{219} (*stick*) forms a tight hydrogen bond with $Asn^{71}{}_{CypA}$ (*stick*). CA_{WT} is shown by a *green ribbon* and the complexed CypA by a *yellow ribbon*; CA_{H219Q} is shown by a *red tube* and the complexed CypA by a *pink tube*. The loss of hydrogen bonds results in reduced CypA incorporation, but there persists sufficient interaction so that there are minimal alterations in the conformation of the CypA binding loop of CA_{151}.

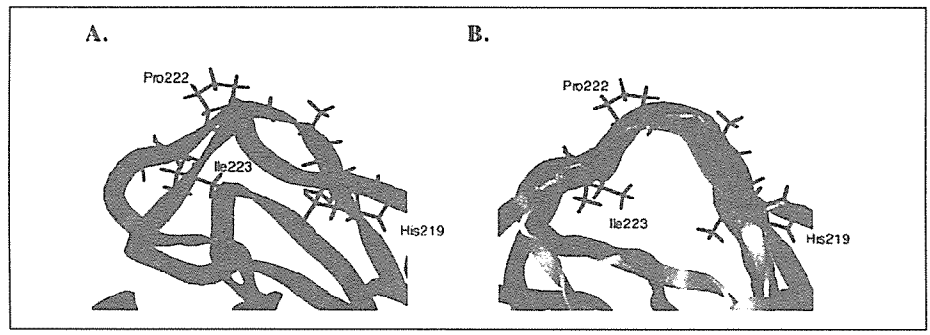

FIGURE 7. **Loop conformations of CA_{WT} and CA_{MT}.** *A*, ribbon diagram of CA_{P222A} (*purple*) superimposed on that of CA_{WT} (*red*). CA_{P222A} causes a significant distortion of the loop structure. The value of weighted root mean square deviation of the structure of CA_{P222A} from CA_{WT} structure is 3.16 Å. *B*, ribbon diagrams of the structures of the CypA binding region of various CA_{MT}, generated with 1-ns dynamics calculations, are superimposed on the structure of CA_{WT}. CA_{WT} is shown in *red*, CA_{H219Q} in *yellow*, CA_{H219P} in *blue*, $CA_{H219Q/P222A}$ in *magenta*, and $CA_{P222A/A224E}$ in *cyan*. *Residues 218–223 of* CA_{WT} are shown as *red sticks*. The values of weighted root mean square deviation of CA_{H219Q}, CA_{H219P}, $CA_{H219Q/P222A}$, and $CA_{P222A/A224E}$ structures from CA_{WT} structure are 0.99, 1.77, 1.24, and 1.48 Å, respectively. H219Q and H219P substitutions do not significantly affect the conformation of the CypA binding region of CA_{WT}. Note that the conformations of the CypA binding region of CA_{WT} and mutant CA species structurally resemble each other. Also note that $CA_{H219Q/P222A}$ and $CA_{P222A/A224E}$ have the conformation of the CypA binding loop region restored close to that of CA_{WT} in comparison with CA_{P222A}.

values of weighted root mean square deviation of CA_{H219Q}, CA_{H219P}, and $CA_{H219Q/P222A}$ structures from CA_{WT} structure were 0.99, 1.77, and 1.24 Å, respectively. Thus, it was thought that the restoration of the distorted conformation of the CypA binding loop caused by H219Q and P222A substitutions were presumably responsible for the improved replication compared with HIV-1_{P222A}, particularly in PHA-PBM where CypA contents are significantly less in comparison with MT-2 and H9 cells (Fig. 3 and Fig. 5, *A–D*).

As noted above, when HIV-1_{1NL4-3} was propagated in the absence of PI in MT-2 cells, the virus also acquired A224V mutation by passage 10 (4). It should be noted that Ala^{224} is also located within the CypA binding loop of p24 Gag protein and is also known to interact with CypA through hydrophobic contacts (9). Therefore, we also examined the highly intriguing findings by Braaten and co-workers (24) that the addition of A224E substitution rescued the replication of an otherwise poorly replicating HIV-1_{P222A} without increasing the level of viral CypA incorporation that had been reduced by P222A substitution. As shown in Fig. 7*B*, the loop conformation, with the two amino acid substitutions, is restored closely to that of the wild-type conformation. The values of weighted root mean square deviation of $CA_{P222A/A224E}$ structure from CA_{WT} structure was 1.48 Å. This observation should corroborate our observation that the conformation of the CypA binding region of capsid is critical for viral fitness.

DISCUSSION

It should be noted that certain polymorphic amino acid residues seen in HIV-1 strains are associated with HIV-1 drug resistance (2, 3). It is also known that certain drug resistance-conferring amino acid substitutions found in one subtype HIV-1 isolated from patients under therapy may be detected in HIV-1 of other subtypes from individuals having received no therapy (25, 26). Moreover, a recent study by Colson *et al.* (27) has revealed that HIV-2 strains harbor specific patterns of natural polymorphism and resistance. It is particularly of note that out of 88 different HIV-1 strains compiled in the HIV Sequence Compendium 2000 (22), 65 had histidine at position 219, whereas13 had glutamine, and 4 had proline. Hence, as studied in this work both Gln^{219} and Pro^{219} represent polymorphic amino acid residues, and it is thought that these

two polymorphic amino acids are associated with the acquisition of resistance to certain PIs.

In the present study, we found that the two substitutions H219Q and H219P were closely associated with replication advantages when propagated in CypA-rich MT-2 and H9 cells. The same advantage was seen in PHA-PBM containing a smaller amount of CypA, but only in a limited fashion (Fig. 2 and Fig. 3, *A* and *B*). We also found that these substitutions reduced CypA incorporation into virions (Fig. 3*C*), which is compatible with previous reports by two groups (28, 29). It was therefore postulated that MT-2 and H9 cells contained high CypA amounts, thereby compromising HIV-1_{WT} replication. However, H219Q and H219P substitutions apparently reduced the viral interaction with CypA, resulting in enhanced HIV-1 replication (Figs. 2 and 3). Most interestingly, when HIV-1_{H219Q} was exposed to CsA (0.5 μM), its replication was suppressed, unlike that of HIV-1_{WT}, and the higher CsA concentration (2.5 μM) further suppressed HIV-1_{H219Q} replication in all the cell preparations examined (Fig. 4). It is noteworthy that Braaten *et al.* (5) reported that virion-associated CypA amounts were reduced by 50 and 75% when HIV-1 was propagated in the presence of 0.5 and 2.5 μM CsA, respectively. Although the exact role of CypA in HIV-1 replication is as yet unclear, CypA seems to play a critical role early in the HIV-1 replication cycle (5, 8, 30) by destabilizing the capsid (p24)-capsid interactions, thereby promoting disassembly of the viral core (9). An excessive depletion of CypA may tighten capsid-capsid binding, thereby interfering with virion uncoating and reducing HIV-1 replication rates, although such a sequel is speculative at present. On the other hand, higher amounts of CypA may greatly destabilize capsid-capsid interactions, thereby rendering the virion core unstable and likewise decrease HIV-1 replication (23). Thus, it was thought that the CsA-induced HIV-1_{H219Q} replication reduction in MT-2 and H9 cells was because of an excessive depletion of CypA. It is also of note that our observation that CsA potentiated HIV-1_{WT} replication in MT-2 and H9 cells, although it failed to boost HIV-1_{H219Q} replication, makes our view more plausible that H219Q substitution is directly responsible for the increased viral replication and the reduction of CypA content in daughter virions.

The presence of Pro at position 222 in p24 Gag protein has been shown to be a primary determinant of CypA binding (9), and its substitution to Ala (P222A) decreases viral CypA incorporation, causing reduced HIV-1 replication in Jurkat cells (5, 6). In this regard, HIV-1_{P222A} was originally reported to have a severely compromised infectivity in Jurkat cells (5, 6), but it was later reported that CypA-rich H9 and CEM cells could support the replication of HIV-1_{P222A} (23, 31). In the present study, we also found that the P222A substitution reduced CypA incorporation by HIV-1 by ~75% (Fig. 5*E*) and significantly reduced HIV-1 replication in Jurkat cells and PHA-PBM, which contained relatively low CypA amounts (Fig. 3, *A* and *B*). We presumed that the introduction of H219Q substitution, which decreases p24 Gag protein binding to CypA (Fig. 3*C*), to HIV-1_{P222A} would further decrease viral CypA incorporation and thereby replication. It was intriguing that the H219Q substitution added to HIV-1_{P222A} potentiated HIV-1 replication as examined in all the cell preparations used (Fig. 5, *A–D*). These data suggest either that the added H219Q substitution enabled HIV-1_{P222A} to incorporate more CypA into daughter virions or altered a conformation of the CypA binding domain of p24 Gag protein, thereby rendering the virus relatively independent of CypA. In fact, the virus-associated CypA amount in HIV-$1_{H219Q/P222A}$ was less than or comparable with that in HIV-1_{P222A} (Fig. 5*E*). It is worth noting that a substitution at position 224 of p24 Gag protein from Ala to Glu (A224E) recovers the compromised replication of HIV-1_{P222A} in Jurkat cells but does not alter the viral CypA incorporation (24). It is also worth noting that even though all the amino acid substitutions examined here decreased viral CypA incorporation, only P222A substitution decreased viral replication. We showed that the loop conformation of the CypA binding region of CA_{WT}, CA_{H219Q}, and CA_{H219P} was quite similar to each other, whereas the conformation of CA_{P222A} sustained the most distortion (Fig. 7, *A* and *B*). It should be noted that $CA_{H219Q/P222A}$ and $CA_{P222A/A224E}$ (24) not only improve viral replication over CA_{P222A} but also restored their conformation (Fig. 5, *A–D*, and Fig. 7, *A* and *B*). We postulate that the conformation of the CypA binding region of CA_{151} is strongly correlated with viral fitness, and the functional role of CypA is to maintain the conformation of CA_{151} for viral replication.

It should be noted that HIV-1 infection of simian cells is restricted at an early post-entry step by the presence of simian TRIM5α (tripartite motif 5α) (32). In this respect, replacement of HIV-1 capsid protein with simian immunodeficiency virus capsid sequence significantly reduced the simian TRIM5α-mediated restrictions, demonstrating that the capsid protein of HIV-1 is a critical viral determinant for susceptibility to post-entry restriction in simian cells (33). Most interestingly, H219Q substitution of HIV-1 capsid is reported to be associated with the reduction of simian TRIM5α-mediated restriction (34, 35), suggesting that conformational change of CypA binding loop by H219Q, as we described in this work, might reduce the recognition by simian TRIM5α. It is also possible that the effects of H219Q observed in this study involve alterations of the interaction of TRIM5α and/or TRIM5α cofactors with the HIV-1 capsid. It is noteworthy that human TRIM5α, which has been shown to partly restrict HIV-1 infection (32), may be contributing to the effects on HIV-1 replication that occur when CypA is not able to bind the capsid protein of HIV-1 (36).

In summary, our study suggests that the H219Q substitution increases HIV-1 replication through (i) maintaining the loop conformation of CypA binding region and (ii) providing favorable conditions for viral replication by reducing viral CypA incorporation. The present data also show that the replication of HIV-1 with $CA_{H219Q/P222A}$ and that with $CA_{P222A/A224E}$, as studied elsewhere (24), were restored as compared with the otherwise compromised replication of HIV-1 with CA_{P222A} by restoring the loop conformation without increasing CypA content. We believe that an optimal concentration of CypA, which is neither excessively high nor excessively low, is critical for viral fitness and that the functional role of CypA is to maintain the conformation of CA_{151}.

Acknowledgments—We are grateful to Douglas Braaten and Jeremy Luban for kindly providing the plasmid of HIV-1_{P222A}; Mark K. Kavlick for technical assistance and helpful discussion; and the Center for Information Technology, National Institutes of Health, for computational resources.

REFERENCES

1. Mitsuya, H., and Erickson, J. (1999) in *Textbook of AIDS Medicine* (Merigan, T. C., Bartlet, J. G., and Bolognesi, D., eds) pp. 751–780, Williams & Wilkins, Baltimore
2. Kavlick, M. F., and Mitsuya, H. (2001) in *Art of Antiretroviral Therapy* (De Clarcq, R., ed) pp. 279–312, American Society for Microbiology, Washington, D. C.
3. Tanaka, M., Srinivas, R. V., Ueno, T., Kavlick, M. F., Hui, F. K., Fridland, A., Driscoll, J. S., and Mitsuya, H. (1997) *Antimicrob. Agents Chemother.* **41,** 1313–1318
4. Gatanaga, H., Suzuki, Y., Tsang, H., Yoshimura, K., Kavlick, M. F., Nagashima, K., Gorelick, R. J., Mardy, S., Tang, C., Summers, M. F., and Mitsuya, H. (2002) *J. Biol. Chem.* **277,** 5952–5961
5. Braaten, D., Franke, E. K., and Luban, J. (1996) *J. Virol.* **70,** 3551–3560
6. Franke, E. K., Yuan, H. E., and Luban, J. (1994) *Nature* **372,** 359–362
7. Braaten, D., and Luban, J. (2001) *EMBO J.* **20,** 1300–1309
8. Steinkasserer, A., Harrison, R., Billich, A., Hammerschmid, F., Werner, G., Wolff, B., Peichl, P., Palfi, G., Schnitzel, W., Mlynar, E., and Rosenwirth, B. (1995) *J. Virol.* **69,** 814–824
9. Gamble, T. R., Vajdos, F. F., Yoo, S., Worthylake, D. K., Houseweart, M., Sundquist,

W. I., and Hill, C. P. (1996) *Cell* **87,** 1285–1294
10. Gross, I., Hohenberg, H., Huckhagel, C., and Krausslich, H. G. (1998) *J. Virol.* **72,** 4798–4810
11. Turner, B. G., and Summers, M. F. (1999) *J. Mol. Biol.* **285,** 1–32
12. Mimoto, T., Imai, J., Kisanuki, S., Enomoto, H., Hattori, N., Akaji, K., and Kiso, Y. (1992) *Chem. Pharm. Bull.* **40,** 2251–2253
13. Kageyama, S., Mimoto, T., Murakawa, Y., Nomizu, M., Ford, H., Shirasaka, T., Gulnik, S., Erickson, J., Takada, K., Hayashi, H., Broder, S., Kiso, Y., and Mitsuya, H. (1993) *Antimicrob. Agents Chemother.* **37,** 810–817
14. Yoshimura, K., Kato, R., Yusa, K., Kavlick, M. F., Maroun, V., Nguyen, A., Mimoto, T., Ueno, T., Shintani, M., Falloon, J., Masur, H., Hayashi, H., Erickson, J., and Mitsuya, H. (1999) *Proc. Natl. Acad. Sci. U. S. A.* **96,** 8675–8680
15. Ghosh, A. K., Kincaid, J. F., Cho, W., Walters, D. E., Krishnan, K., Hussain, K. A., Koo, Y., Cho, H., Rudall, C., Holland, L., and Buthod, J. (1998) *Bioorg. Med. Chem. Lett.* **8,** 687–690
16. Yoshimura, K., Kato, R., Kavlick, M. F., Nguyen, A., Maroun, V., Maeda, K., Hussain, K. A., Ghosh, A. K., Gulnik, S. V., Erickson, J. W., and Mitsuya, H. (2002) *J. Virol.* **76,** 1349–1358
17. Kimpton, J., and Emerman, M. (1992) *J. Virol.* **66,** 2232–2239
18. Kosalaraksa, P., Kavlick, M. F., Maroun, V., Le, R., and Mitsuya, H. (1999) *J. Virol.* **73,** 5356–5363
19. Tamiya, S., Mardy, S., Kavlick, M. F., Yoshimura, K., and Mitsuya, H. (2004) *J. Virol.* **78,** 12030–12040
20. Kaminski, G. A., Friesner, R. A., Tirado-Rives, J., and Jorgensen, W. J. (2001) *J. Phys. Chem.* **105,** 6474–6487
21. Still, W. C., Tempczyk, A., Hawley, R. C., and Hendrickson, T. (1990) *J. Am. Chem. Soc.* **112,** 6127–6129
22. Kuiken, C., Foley, B., Hahn, B., Marx, P., McCutchan, F., Mellors, J. W., Mullins, J., Wolinsky, S., and Korber, B. (2000) in *Human Retroviruses and AIDS* (Bradac, J., ed) pp. 201–298, Los Alamos National Laboratory, Los Alamos, NM
23. Yin, L., Braaten, D., and Luban, J. (1998) *J. Virol.* **72,** 6430–6436
24. Braaten, D., Aberham, C., Franke, E. K., Yin, L., Phares, W., and Luban, J. (1996) *J. Virol.* **70,** 5170–5176
25. Cornelissen, M., van den Burg, R., Zorgdrager, F., Lukashov, V., and Goudsmit, J. (1997) *J. Virol.* **71,** 6348–6358
26. Quinones-Mateu, M. E., Albright, J. L., Mas, A., Soriano, V., and Arts, E. J. (1998) *J. Virol.* **72,** 9002–9015
27. Colson, P., Henry, M., Tourres, C., Lozachmeur, D., Gallais, H., Gastaut, J. A., Moreay, J., and Tamalet, C. (2004) *J. Clin. Microbiol.* **42,** 570–577
28. Li, Q., Moutiez, M., Charbonnier, J. B., Vaudry, K., Menez, A., Quemeneur, E., and Dugave, C. (2000) *J. Med. Chem.* **43,** 1770–1779
29. Yoo, S., Myszka, D. G., Yeh, C., McMurray, M., Hill, C. P., and Sundquist, W. I. (1997) *J. Mol. Biol.* **269,** 780–795
30. Thali, M., Bukovsky, A., Kondo, E., Rosenwirth, B., Walsh, C. T., and Sodroski, J. (1994) *Nature* **372,** 363–365
31. Ackerson, B., Rey, O., Canon, J., and Krogstad, P. (1998) *J. Virol.* **72,** 303–308
32. Stremlau, M., Owens, C. M., Perron, M. J., Kiessling, M., Autissier, P., and Sodroski, J. (2004) *Nature* **427,** 848–853
33. Owens, C. M., Yang, P. C., Göttlinger, H., and Sodroski, J. (2003) *J. Virol.* **77,** 726–731
34. Owens, C. M., Song, B., Perron, M. J., Yang, P. C., Stremlau, M., and Sodroski, J. (2004) *J. Virol.* **78,** 5423–5437
35. Kootstra, N. A., Münk, C., Tonnu, N., Landau, N. R., and Verma, I. M. (2003) *Proc. Natl. Acad. Sci. U. S. A.* **100,** 1298–1303
36. Towers, G. J., Hatziioannou, T., Cowan, S., Goff, S. P., Luban, J., and Bieniasz, P. D. (2003) *Nat. Med.* **9,** 1138–1143

THE JOURNAL OF BIOLOGICAL CHEMISTRY VOL. 281, NO. 18, pp. 12688–12698, May 5, 2006
Printed in the U.S.A.

Structural and Molecular Interactions of CCR5 Inhibitors with CCR5*

Received for publication, November 28, 2005, and in revised form, January 25, 2006 Published, JBC Papers in Press, February 23, 2006, DOI 10.1074/jbc.M512688200

Kenji Maeda[‡§¶], Debananda Das[¶], Hiromi Ogata-Aoki[‡§], Hirotomo Nakata[‡§], Toshikazu Miyakawa[§], Yasushi Tojo[‡§], Rachael Norman[¶], Yoshikazu Takaoka[‖], Jianping Ding[**], Gail F. Arnold[**], Eddy Arnold[**], and Hiroaki Mitsuya[‡§¶1]

From the [‡]Department of Hematology and [§]Department of Infectious Diseases, Kumamoto University Graduate School of Medical and Pharmaceutical Sciences, Kumamoto 860-8556, Japan, the [¶]Experimental Retrovirology Section, HIV and AIDS Malignancy Branch, NCI, National Institutes of Health, Bethesda, Maryland 20892, the [‖]Minase Research Institute, Ono Pharmaceutical Co. Ltd., Osaka 618-8585, Japan, and the [**]Center for Advanced Biotechnology and Medicine, and Chemistry and Chemical Biology Department, Rutgers University, Piscataway, New Jersey 08854

We have characterized the structural and molecular interactions of CC-chemokine receptor 5 (CCR5) with three CCR5 inhibitors active against R5 human immunodeficiency virus type 1 (HIV-1) including the potent *in vitro* and *in vivo* CCR5 inhibitor aplaviroc (AVC). The data obtained with saturation binding assays and structural analyses delineated the key interactions responsible for the binding of CCR5 inhibitors with CCR5 and illustrated that their binding site is located in a predominantly lipophilic pocket in the interface of extracellular loops and within the upper transmembrane (TM) domain of CCR5. Mutations in the CCR5 binding sites of AVC decreased gp120 binding to CCR5 and the susceptibility to HIV-1 infection, although mutations in TM4 and TM5 that also decreased gp120 binding and HIV-1 infectivity had less effects on the binding of CC-chemokines, suggesting that CCR5 inhibition targeting appropriate regions might render the inhibition highly HIV-1-specific while preserving the CC chemokine-CCR5 interactions. The present data delineating residue by residue interactions of CCR5 with CCR5 inhibitors should not only help design more potent and more HIV-1-specific CCR5 inhibitors, but also give new insights into the dynamics of CC-chemokine-CCR5 interactions and the mechanisms of CCR5 involvement in the process of cellular entry of HIV-1.

Highly active antiretroviral therapy has brought about a major impact on the acquired immunodeficiency syndrome (AIDS) epidemics in industrially advanced nations (1, 2), however, eradication of HIV-1[2] appears to be currently impossible mainly because of the viral reservoirs remaining in blood and infected tissues (3). Successful antiviral drugs, in theory, exert their virus-specific effects by interacting with viral components such as viral genes or their transcripts without disturbing cellular metabolisms or functions (2). However, at present, no antiretroviral drugs or agents have been demonstrated to be completely specific for HIV-1 and devoid of toxicity or side effects in the therapy of AIDS (4). Limitations of antiviral therapy of AIDS are exacerbated by complicated regimens, emergence of drug-resistant HIV-1 variants (1), and a number of inherent adverse effects (5).

Thus, identification of new antiretroviral drugs that have unique mechanisms of action and produce no or least minimal side effects remains an important therapeutic objective (2, 4). CCR5 is a member of the G protein-coupled, seven-transmembrane segment receptors, which comprise the largest superfamily of proteins in the body (6). In 1996, it was revealed that CCR5 serves as one of the two essential coreceptors for HIV-1 entry to human $CD4^+$ cells, thereby serving as an attractive target for possible intervention of HIV-1 infection (7–10). Aplaviroc (AVC; AK602/ONO4128/873140; Fig. 1), a novel spirodiketopiperazine derivative, represents a CCR5 inhibitor that specifically binds to human CCR5 with a high affinity, greatly blocks HIV-1-gp120/CCR5 binding, and exerts potent activity against a wide spectrum of laboratory and primary R5-HIV-1 isolates including multidrug-resistant $HIV\text{-}1_{MDR}$ (IC_{50} values of 0.2–0.6 nM) (11). AVC, despite its much greater anti-HIV-1 activity than other previously published CCR5 inhibitors including TAK-779 and SCH-C (Fig. 1), preserves RANTES and macrophage inflammatory protein-1β binding to $CCR5^+$ cells and their functions, whereas TAK-779 and SCH-C fully block the CC-chemokines/CCR5 interactions (11). AVC reportedly has an extensive and prolonged CCR5 occupancy as examined in phytohemagglutinin-activated peripheral blood mononuclear cells ($t_{1/2} \sim 9$ h) (12) and in circulating lymphocytes in HIV-1-negative and HIV-1-positive individuals ($t_{1/2}$ of 69–152 h depending on different AVC doses) (37). In a randomized, placebo-controlled short-term monotherapy trial in patients with AIDS including those who were drug-experienced, AVC demonstrated potent antiretroviral activity and brought about significant reduction in HIV-1 viremia (by ~1.7 log) in AIDS patients (38).

In the present study, we examined the profile of binding to and interactions with CCR5 of three CCR5 inhibitors, AVC, SCH-C, and TAK-779. We also conducted structural analyses of the interactions of CCR5 inhibitors with CCR5, using homology modeling, robust structure refinement, and docking. Notably, the molecular modeling analyses were combined and fine-tuned with the results of the saturation binding assay using a panel of mutant CCR5-expressing cells and [^{3}H]CCR5 inhibitors and the resultant configurations and orientations of inhibitors docked within the hydrophobic cavity of CCR5 yielded structure-activity predictions and interpretations consistent with the observed experimental data. The present approach of combining the site-directed mutagenesis-based data and molecular modeling should represent a

* This work was supported in part by the Intramural Research Program of the Center for Cancer Research, NCI, National Institutes of Health, and in part by a grant-in-aid for Scientific Research (Priority Areas) from the Ministry of Education, Culture, Sports, Science, and Technology of Japan (Monbu-Kagakusho), a Grant for Promotion of AIDS Research from the Ministry of Health, Welfare, and Labor of Japan Kosei Rohdosho H15-AIDS-001, and the Cooperative Research Project on Clinical and Epidemiological Studies of Emerging and Re-emerging Infectious Diseases (Renkei Jigyo number 78, Kumamoto University) of Monbu-Kagakusho. The costs of publication of this article were defrayed in part by the payment of page charges. This article must therefore be hereby marked "*advertisement*" in accordance with 18 U.S.C. Section 1734 solely to indicate this fact.

[1] To whom correspondence should be addressed. Tel.: 81-96-373-5156; Fax: 81-96-363-5265; E-mail: hmitsuya@helix.nih.gov.

[2] The abbreviations used are: HIV-1, human immunodeficiency virus, type 1; AVC, aplaviroc; CCR5, CC-chemokine receptor 5; MIP-1α, macrophage inflammatory protein-1α; RANTES, regulated upon activation, normal T cell expressed and secreted; CHO, Chinese hamster ovary; FCS, fetal calf serum; mAb, monoclonal antibody; TM, transmembrane; gp, glycoprotein.

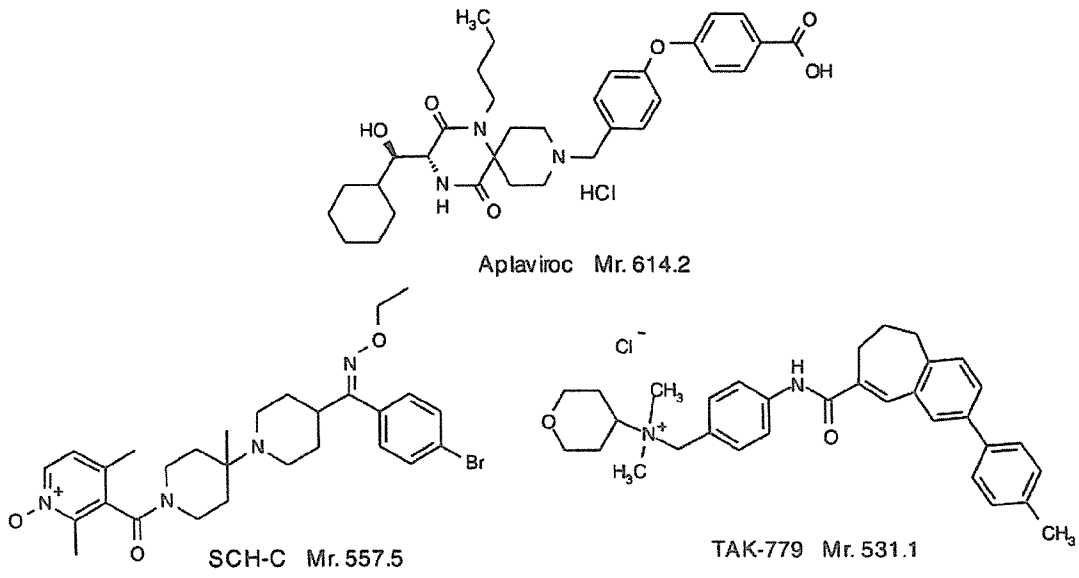

FIGURE 1. **Structures of AVC, TAK-779, and SCH-C.**

valuable strategy for gaining structural insights for membrane-bound proteins for which x-ray crystal structures are not as yet available. The present data delineating residue by residue interactions of CCR5 with CCR5 inhibitors should not only help design more potent and more HIV-1-specific CCR5 inhibitors, but also give new insights into the dynamics of CC-chemokine-CCR5 interactions and the mechanisms of CCR5 involvement in the process of cellular entry of HIV-1.

EXPERIMENTAL PROCEDURES

Reagents—A CCR5 inhibitor, AVC, was designed and synthesized as previously published (11). Two other CCR5 inhibitors, TAK-779 and SCH-351125 (SCH-C), were synthesized based on the previously published structures (13, 14) (Fig. 1). These three CCR5 inhibitors were tritiated by reductive amination with sodium triacetoxyborotritide (15), methylation with [^{3}H]methyliodide, and/or heterogeneous catalytic exchange with tritium gas (16). Two ^{125}I-labeled chemokines (macrophage inflammatory protein-1α (MIP-1α) and regulated upon activation, normal T cell expressed and secreted (RANTES)) were purchased from Amersham Biosciences and ^{125}I-labeled macrophage inflammatory protein-1β (MIP-1β) was purchased from PerkinElmer Life Sciences, Inc. Their corresponding unlabeled chemokines were purchased from PeproTech Inc. (Rocky Hill, NJ). Recombinant HIV-1_{YU2} gp120 (rgp120) and human soluble CD4 (sCD4) were purchased from Immuno Diagnostics, Inc. (Woburn, MA).

Cells and Viruses—The Chinese hamster ovary (CHO) cells overexpressing CCR5 (17) were maintained in Ham's F-12 medium (Invitrogen) supplemented with 10% fetal calf serum (FCS: JRH Biosciences, Lenaza, KS) and 50 units/ml penicillin and 50 μg/ml streptomycin in the presence of 5 μg/ml blasticidin S hydrochloride. The HeLa-CD4-LTR-β-galactosidase indicator cell line expressing human CCR5 (CCR5$^+$MAGI (multinuclear activation of galactosidase indicator) cells) (18) was a kind gift from Dr. Yosuke Maeda, Kumamoto University Graduate School of Medical and Pharmaceutical Sciences, Japan. CCR5$^+$MAGI cells were maintained in Dulbecco's modified Eagle's medium (DMEM) supplemented with 10% FCS, 200 μg/ml G418, 100 μg/ml hygromycin B, and 100 μg/ml zeomycin. The U373-MAGI cell line was obtained from the AIDS Research and Reference Reagent Program, NIAID, National Institutes of Health (Bethesda, MD). U373-MAGI cells were maintained in Dulbecco's modified Eagle's medium supplemented with 10% FCS, 200 μg/ml G418, and 100 μg/ml hygromycin B. An R5-HIV-1 strain, HIV-1_{BaL}, was employed for the determination of the susceptibility of mutant CCR5 (CCR5$_{MT}$)-expressing cells to the infectivity of HIV-1.

Generation of Wild-type and CCR5$_{MT}$-overexpressing Cells—A mammalian expression vector pZeoSV2 (Invitrogen) carrying the human wild-type *CCR5* (*CCR5$_{WT}$*) gene (pZeoSV-*CCR5*) (18) was a kind gift from Dr. Yosuke Maeda. A variety of plasmids carrying a mutant *CCR5*-encoding gene were generated using the site-directed mutagenesis technique employing the QuikChange site-directed mutagenesis kit (Stratagene, La Jolla, CA) as described by the manufacturer. Mutations introduced into the *CCR5* gene were introduced through: (i) substitution of an amino acid(s) or (ii) deletion of an amino acid(s) at selected amino acid positions of CCR5. A mutation from Gly to Arg at position 163, where the corresponding amino acid in simian CCR5 is Arg, was also introduced. This G163R substitution has been reported to reduce the binding of R5-HIV-1-gp120 to human CCR5 and the susceptibility to HIV-1 (19). All these plasmids were confirmed to contain only the desired mutation(s) by nucleotide sequencing.

CHO cells (or U373-MAGI cells) were transfected with a plasmid containing the *CCR5$_{WT}$*-encoding gene or a plasmid carrying a *CCR5$_{MT}$*-encoding gene using Lipofectamine (Invitrogen); the transfectants were magnetically sorted, following treatment with an anti-CCR5 monoclonal antibody (2D7 or 3A9; BD Pharmingen, San Diego, CA), using Dynabeads M-450 coupled to goat anti-mouse IgG (Dynal A.S., Oslo, Norway); and the cells were cloned using the limiting dilution technique.

Determination of CCR5 Expression Levels in CHO and U373-MAGI Cells—CCR5 expression levels of the various clones described above were determined using three indicators: (i) maximal amounts of [^{3}H]AVC bound to cells (B_{max}); (ii) mean florescence intensity values when stained with monoclonal antibody (mAb) 3A9; and (iii) mean florescence intensity values when stained with mAb 2D7. The antigenic epitope for 2D7 is located distant from that for 3A9 (20) and 3A9 does not compete with AVC binding to CCR5 (data not shown). The expression levels were expressed as % control (CCR5$_{WT}$-expressing cells as control), and the highest value obtained was chosen as the estimated

CCR5 expression level. There were no clones that had low values in all three indicators, thus sustaining that the current method used for the CCR5 expression levels was thought to be legitimate. CD4 and CCR5 expression levels were also determined using the quantitative fluorescence-activated cell sorting assay system (Quantum Simply Cellular Kit; Sigma) using 3A9 and 2D7 (12). For the HIV-1 susceptibility assay, U373-MAGI clones that expressed CD4 molecules ranging 10–25 × 10^4 antigen-binding sites were selected. $CCR5_{MT}$-expressing CHO cells were maintained in Ham's F-12 medium containing 10% FCS and 100 μg/ml zeomycin. $CCR5_{WT}$- and $CCR5_{MT}$-expressing U373-MAGI cells were cultured in Dulbecco's modified Eagle's medium supplemented with 10% FCS, 200 μg/ml G418, 100 μg/ml hygromycin B, and 100 μg/ml zeomycin.

Saturation Binding Assay Using ^{3}H-Labeled CCR5 Inhibitors—Saturation binding assay using ^{3}H-labeled CCR5 inhibitors was conducted and the K_D values of CCR5 inhibitors in $CCR5_{WT}$-, or $CCR5_{MT}$-expressing CHO cells were calculated as previously described (11).

Radiolabeled Inhibitor Binding/Competition Studies—$CCR5_{WT}$-expressing cells (1.5 × 10^5) were plated onto 48-well microculture plates, incubated for 24 h, rinsed, exposed to [^{3}H]AVC, [^{3}H]SCH-C, or [^{3}H]TAK-779 for 15 min at room temperature, subsequently exposed to various concentrations of unlabeled CCR5 inhibitors, incubated for 30 min, thoroughly washed, lysed, and the radioactivity in the lysates was counted. All experiments were performed in duplicate. The amounts of each ^{3}H-labeled CCR5 inhibitor bound to the cells are shown as mean % control values. Standard deviation values are indicated with the vertical lines. To obtain control values, the experiment was also performed without the addition of unlabeled CCR5 inhibitors.

Determination of CC-chemokine- and HIV-1 Gp120 Binding Affinity to $CCR5_{WT}$ and $CCR5_{MT}$—Binding profiles of chemokines to $CCR5_{WT}$- or $CCR5_{MT}$-expressing cells were determined using ^{125}I-labeled chemokines as previously reported (11) with minor modifications. In brief, $CCR5_{WT}$- or $CCR5_{MT}$-expressing cells (1.5 × 10^5) were plated onto 48-well microculture plates, incubated for 24 h, rinsed, exposed to 5 nM ^{125}I-MIP-1α, ^{125}I-MIP-1β, or ^{125}I-RANTES at room temperature for 1 h, thoroughly washed with phosphate-buffered saline, lysed with 0.5 ml of 1 N NaOH, and the radioactivity in the lysates counted. The nonspecific binding of the labeled chemokine to the cells was determined based on the radioactivity detected in the wells plated with the same number of CCR5-negative CHO (CHO-K1) cells exposed to an equal amount of ^{125}I-labeled chemokine. Determination of the binding profiles of HIV-1-rgp120 to $CCR5_{WT}$ or $CCR5_{MT}$ was also conducted. Briefly, $CCR5^+$CHO cells were exposed to rgp120 (5 μg/ml) and sCD4 (5 μg/ml: biotinylated using EZ-link sulfo-NHS-SS-biotin (Pierce)) for 1 h at 37 °C. Cells were washed and binding of the rgp120-sCD4 complex to $CCR5^+$CHO cells was determined using phycoerythrin-conjugated streptavidin (SA-PE: BD Pharmingen). Nonspecific binding was determined based on the mean florescence intensity of SA-PE with sCD4 but without rgp120. Because CCR5 expression levels vary among CCR5 clones, the % binding (occupancy) values for ^{125}I-chemokines and rgp120 were normalized using the following formula: % binding (occupancy) = 100 × (amount of ^{125}I-chemokine or rgp120 bound to $CCR5_{MT}$/amount of ^{125}I-chemokine or rgp120 bound to $CCR5_{WT}$) × (number of $CCR5_{WT}$/number of $CCR5_{MT}$), where numbers of $CCR5_{WT}$ and $CCR5_{MT}$ are expressed as B_{max} (cpm) or mean florescence intensity values as described above.

Determination of HIV-1 Susceptibility of $CCR5_{WT}$- and $CCR5_{MT}$-expressing Cells—The susceptibility of $CCR5_{WT}$- and $CCR5_{MT}$-expressing cells to the infection by an R5-HIV-1 strain, $HIV\text{-}1_{BaL}$, was determined as previously described (22). In brief, target cells ($CCR5_{WT}$- or $CCR5_{MT}$-expressing U373-MAGI cells; 10^4/well) were plated onto 96-well flat microtiter culture plates, inoculated with 100 $TCID_{50}$ of $HIV\text{-}1_{BaL}$ on the following day, cultured for 48–72 h, stained with 400 μg/ml of 5-bromo-4-chloro-3-indolyl-β-D-galactopyranoside (X-gal), and all blue cells were counted. All experiments were performed in triplicate. For testing each $CCR5_{MT}$-expressing cell preparation, multiple (5 to 13) clones were examined. In each set of experiments, $CCR5_{WT}$-clone 1 was included and served as a standard. Percent infection in $CCR5_{WT}$- and $CCR5_{MT}$-expressing cells was determined using the following formula: % Infection = 100 × (mean blue cell number in a well)/(mean blue cell number in a well of $CCR5_{WT}$-clone 1).

Structural Modeling of the Interactions of CCR5 Inhibitors with Wild-type and Mutant CCR5 Species—An initial structural model of CCR5 was defined with homology modeling using the crystal structure of bovine rhodopsin as a template (23). This resulted in the initial placement of the helices and side chains. The CCR5-inhibitor complex structures were defined with an iterative optimization of CCR5 and inhibitor structures in the presence of each other, using software tools from Schrödinger (Schrödinger, LLC, New York), as described below. The conformational flexibility of both CCR5 and the inhibitors were taken into account. The molecular structures of AVC, SCH-C, and TAK-779, without the presence of counter-ions and solvents, were obtained by minimization using the MMFF94 force field (24). For each minimized inhibitor configuration, a set of low energy structures was generated by performing a Monte Carlo sampling of their conformations. Thus obtained structures were used as starting structures for docking calculations where their conformations were further refined.

The protonation states of CCR5 residues were assigned, and residues more than 20 Å from the active site were neutralized. In an attempt to place an inhibitor within CCR5, initially the active site was artificially enlarged by mutating Tyr^{108}, Cys^{178}, Glu^{283}, and Met^{287} to Ala. The van der Waals radii of inhibitor atoms were scaled by a factor of 0.70 to reduce steric clashes and docked into CCR5. After obtaining an initial set of CCR5-inhibitor complexes, residues 108, 178, 283, and 287 were mutated back from Ala to their original states. CCR5 atoms within 15 Å of an initially placed inhibitor were subsequently refined. It was achieved by using the rotamer library of Xiang and Honig (25) and optimizing each side chain one at a time holding all other side chains fixed. After convergence, all side chains were simultaneously energy minimized using the OPLS-AA force field (26) to remove any remaining clashes. The inhibitors were docked again and scored to estimate their relative affinity. The docked complexes with higher scores were visually examined along with the mutational data to select the best possible CCR5-inhibitor complex.

Mutated CCR5 structures were defined using the wild-type CCR5 structure and optimized using the OPLS2003 force field. Charges were taken from the force field. The minimization was carried out until the gradient was below 0.2 kJ/Å-mol. Resulting minimized structures were used as starting structures for obtaining docked complexes of mutated CCR5 with inhibitors using the protocol described above. Visualization, structural refinement, and docking were performed using Maestro 7.0, MacroModel 9.0, Prime 1.2, Glide 3.5, and IFD script from Schrödinger, LLC (New York). The extra precision mode of Glide, which has higher penalties for unfavorable and unphysical interactions, was used (27). Computations were carried out on a multiprocessor SGI Origin 3400 computer platform.

A probe radius of 1.4 Å with Connolly surfaces generated was used to define binding site cavities using the method of Exner *et al.* (28) as implemented in the MOLCAD tool in Sybyl 7.0 (Tripos, Inc., St. Louis,

TABLE 1
Binding affinity of CCR5 inhibitors to mutant CCR5s

Mutant CCR5 overexpressed on CHO cells		K_D value[a]			Gp120/sCD4 binding[b]
		Aplaviroc	SCH-C	TAK-779	
			nM		% control
Wild type		2.9 ± 1.0	16.0 ± 1.5	30.2 ± 7.6	100 ± 13.3
D11A	NH_2 terminus	3.0 ± 0.6	12.4 ± 2.0	24.5 ± 3.7	35.4 ± 4.7
Y37A	TM1	7.9 ± 0.9	>200	**98.9 ± 11.5**	35.4 ± 3.7
Y108A		**19.8 ± 4.4**[c]	11.8 ± 1.1	>200	13.2 ± 1.0
F112L		4.0 ± 2.6	30.0 ± 6.4	33.0 ± 7.2	
F112Y	TM3	6.8 ± 1.1	35.8 ± 7.6	28.5 ± 3.1	111 ± 6.9
F113A		**13.3 ± 2.3**	43.8 ± 6.3	32.7 ± 3.3	
F113Y		8.6 ± 3.4	45.3 ± 12.1	32.4 ± 3.0	
G163A	TM4-ECL2[d]	8.0 ± 4.2	25.0 ± 8.2	24.0 ± 5.9	
G163R		>200	46.3 ± 16.5	88.3 ± 22.9	34.1 ± 5.4
R168A		**13.2 ± 3.3**	21.0 ± 8.1	43.0 ± 4.7	
K171A/E172A		2.8 ± 0.1	34.8 ± 6.8	30.5 ± 0.7	29.6 ± 2.2
C178A		>200	27.1 ± 4.4	34.5 ± 3.5	20.9 ± 1.0
S180A		5.7 ± 1.2	31.8 ± 14.4	18.2 ± 3.2	
S180T	ECL2	1.5 ± 0.6	25.4 ± 6.8	41.0 ± 3.8	101 ± 15.0
S180E		**13.9 ± 1.7**	16.5 ± 2.2	25.0 ± 3.5	51.6 ± 1.1
Y184A/S185A		2.0 ± 0.8	21.3 ± 5.0	28.0 ± 2.5	
Y184A/S185A/Q186A/Y187A		2.0 ± 0.6	14.9 ± 0.6	32.3 ± 5.8	
Q186A/Y187A		2.8 ± 0.5	14.7 ± 8.8	35.2 ± 5.8	
Q188A		6.6 ± 1.4	23.8 ± 1.5	37.9 ± 2.5	
WKNF190del		>200	**49.2 ± 1.7**	80.1 ± 16.7	
K191A		>200	26.5 ± 7.1	35.0 ± 3.8	45.7 ± 0.6
K191R	ECL2-TM5	**9.0 ± 5.6**	34.1 ± 19.1	47.1 ± 8.8	
K191N		**14.2 ± 1.1**	35.8 ± 9.2	35.1 ± 9.3	
K197A	TM5	**9.2 ± 4.3**	16.8 ± 2.9	14.7 ± 1.1	
I198A		**24.6 ± 4.8**	**52.4 ± 3.0**	54.9 ± 6.9	51.7 ± 3.0
Y251A	TM6	**36.5 ± 9.5**	21.5 ± 8.6	43.0 ± 4.5	14.5 ± 0.7
E283A		>200	>200	>200	4.3 ± 0.6
M287A	TM7	6.8 ± 2.3	28.0 ± 9.1	39.8 ± 7.5	104 ± 3.9
M287E		**14.8 ± 1.7**	32.2 ± 4.2	53.1 ± 3.7	22.0 ± 0.8

[a] K_D values were determined using saturation binding assays ("Experimental Procedures").
[b] Gp120/sCD4 binding affinity to $CCR5_{MT}$ is shown by % control (see "Experimental Procedures" for reference); the data are also shown in Fig. 8A.
[c] K_D values more than 3-fold compared to that with $CCR5_{WT}$ are shown in bold. All K_D values were determined on multiple occasions (twice to 6 times). Considering the standard deviation for the wild type and other mutations, a 3-fold difference was seen to be statistically significant.
[d] ECL, extracellular loop.

MO). Lipophilic potential was mapped onto the cavities using parameters from Viswanadhan *et al.* (29).

RESULTS

Site-directed Mutagenesis of CCR5 and Binding Affinity of CCR5 Inhibitors—We have previously reported (11) that AVC competitively blocked the binding of a monoclonal antibody, 45531, which is known to be specific against the C-terminal half (or domain B) of the second extracellular loop (ECL2B) of CCR5 (21), whereas AVC failed to block or only partially blocked the binding of two other monoclonal antibodies, 2D7 and 45523, specific for CCR5 but not for its ECL2B. When we examined three additional monoclonal antibodies, 3A9 and 45502 (both specific for NH_2 terminus) and 45549 (multidomain reactive) (20, 21), none of these antibodies were replaced by AVC (data not shown). These data suggest that the potent inhibitory activity of AVC against R5 HIV-1 infection stems from its binding to ECL2B and/or its vicinity with high affinity.

In an attempt to delineate the CCR5 binding profile of the three CCR5 inhibitors, we generated a variety of CCR5 mutant-overexpressing ($CCR5_{MT}$) CHO cells and determined the K_D values of each inhibitor to mutant CCR5 species using the saturation binding assay with tritiated inhibitors. When we determined the K_D value of AVC with respect to a CCR5 mutant carrying an Asp to Ala substitution at position 11 of the amino terminus domain ($CCR5_{D11A}$), the value was 3.0 nM, virtually identical to the K_D value with wild-type CCR5 ($CCR5_{WT}$; Table 1), indicating that the D11A substitution did not affect the binding of AVC to CCR5. The K_D value of AVC with respect to $CCR5_{Y37A}$ was moderately greater with 7.9 nM (2.7-fold compared with the K_D value with regard to $CCR5_{WT}$). On the other hand, those of TAK-779 and SCH-C to $CCR5_{Y37A}$ were 98.9 nM (3.3-fold compared with the K_D with regard to $CCR5_{WT}$) and >200 nM (>12.5-fold), respectively, in agreement with the previous reports in which both TAK-779 and SCH-C apparently failed to bind, probably explaining that these inhibitors failed to block HIV-1 infection of $CCR5_{Y37A}$-expressing cells (30, 31). These data suggest that the binding of TAK-779 and SCH-C to $CCR5_{WT}$ is more dependent on interactions with Tyr37 than that of AVC. We also generated a series of CCR5-overexpressing CHO cells carrying a mutation(s) at a selected amino acid position(s). As shown in Table 1, the mutations that substantially (more than 3-fold compared with AVC binding to $CCR5_{WT}$) affected the K_D values of AVC were as follows: Y108A and F113A in the third transmembrane domain (TM3) of CCR5; R168A and S180E in ECL2; K191R and K191N of the interface of ECL2B and TM5; K197A and I198A of TM5; Y251A of TM6; and M287E of TM7. The mutations that greatly diminished the binding of AVC (values of >200 nM) to CCR5 were as follows: G163R, C178A, WKNF190del, K191A, and E283A. It is worthwhile to interject that Lys^{191} in ECL2 is reported to be critical for the binding of RANTES, MIP-1α, and MIP-1β to CCR5 (32, 33), whereas Cys^{178} is presumed to form a disulfide bond with Cys^{101} of ECL1 and to be critical for the conformation of CCR5 (34). Mutations that substantially affected the binding of TAK-779 and SCH-C to CCR5 were as follows: Y37A, Y108A, and E283A for TAK-779; and Y37A, WKNF190del, I198A, and E283A for SCH-C. It is noteworthy that the number of mutations that affected the binding of AVC was notably greater than those of TAK-779 and SCH-C. Thus, the CCR5 binding modes of AVC, TAK-779, and SCH-C apparently share some similar features but also have some distinct differences.

Structural Analysis Locates Aplaviroc in the Interface of ECL and TM Domains—In the present study, a three-dimensional model of human CCR5-CCR5 inhibitor complex was defined by combining the results of site-directed mutagenesis-based analyses (Table 1) and molecular modeling that involved structure refinement and simultaneous docking of inhibitors to an initial structure of CCR5 based on the crystal structure of bovine rhodopsin (23). Fig. 2 illustrates the three-dimensional model of CCR5 that has a seven-transmembrane helical structure. Six hydrophobic cavities were identified in the extracellular, transmembrane, and intracellular domains of CCR5. Among them, a hydrophobic cavity to which CCR5 inhibitors highly likely to bind was identified based on its size and location (*red arrowhead* in Fig. 2). This cavity is the largest one among the six that can accommodate a molecule of the size of AVC and other CCR5 inhibitors and is in the region implicated to have the greatest effect on K_D values with amino acid substitutions introduced in CCR5 among the six hydrophobic cavities identified. It should be noted, however, that the conformations of CCR5 without an inhibitor and CCR5 with the inhibitor can be substantially different from each other, because significant conformational changes would be expected to follow ligand binding to CCR5. Nevertheless, it is intriguing to note that this largest cavity corresponds to the binding site for the retinal ligand in bovine rhodopsin; given the propensity of this pocket to bind fairly large ligands such as the CCR5 inhibitors, it is possible that this binding cavity could accommodate some as-yet uncharacterized ligands produced in the body during the normal function of CCR5, potentially even some with regulatory roles.

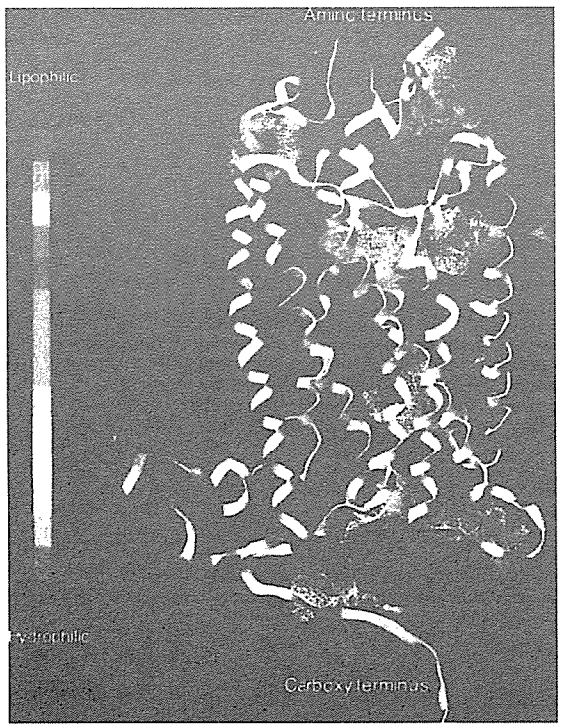

FIGURE 2. **Hydrophobic cavities identified within CCR5.** Six hydrophobic cavities are identified within human CCR5, defined using MOLCAD (Sybyl 7.0). Note the largest hydrophobic cavity (*red arrowhead*) that is likely to accommodate a molecule of the size of AVC and other CCR5 inhibitors and is in the region implicated to have greatest effects on K_D values (see mutagenesis-based results in Table 1).

Based on the set of the K_D values of AVC in relation to various mutant CCR5 species overexpressed on CHO cells (Table 1), structural analysis of AVC-CCR5 interactions was conducted, which suggested that a series of intramolecular and intermolecular hydrogen bonds occur, which should stabilize the CCR5-AVC complex. We identified a significant network of hydrogen bonds among four amino acid residues: Gly^{163}, Ser^{180}, Lys^{191}, and Thr^{195} (Fig. 3*A*). Gly^{163} is located in TM4, Ser^{180} in ECL2, and Lys^{191} and Thr^{195} in TM5. Another network of hydrogen bonds was identified among another four amino acid residues: Tyr^{37}, Glu^{283}, Met^{287}, and Tyr^{108} (Fig. 3*B*). Tyr^{37} is located in TM1, Tyr^{108} in TM3, and Glu^{283} and Met^{287} in TM7. These hydrogen bond networks spanning multiple domains appear to maintain the optimal shape of the cavity for the binding of AVC. Indeed, further analysis of the cavity also revealed that the ECL regions have some hydrophilic characters (Fig. 4*A*, *red arrowhead*), whereas the rest of the cavity is mostly lipophilic (Fig. 4*A*). The carboxyl and hydroxymethyl of AVC interact with the hydrophilic regions of CCR5. The rest of AVC inter-

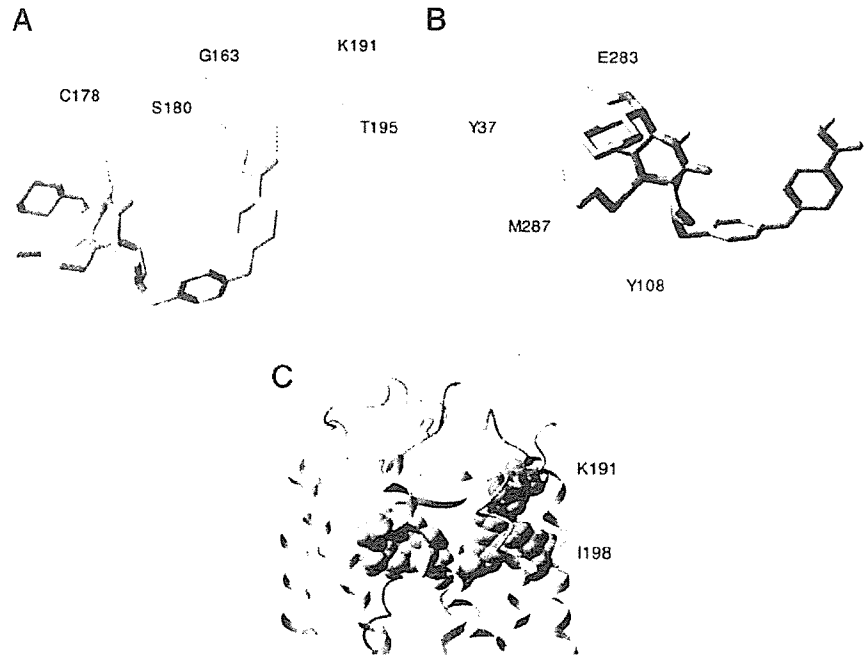

FIGURE 3. **Hydrogen bond networks within CCR5 critical for AVC binding to CCR5.** The structure of the CCR5-AVC complex was defined with iterative structural refinement using docking and homology modeling. Only polar hydrogen atoms are shown. *Panel A*, an intramolecular hydrogen bond network comprised of Gly^{163}, Ser^{180}, Lys^{191}, and Thr^{195} is seen. Gly^{163} is located in TM4, Ser^{180} in ECL2, and Lys^{191} and Thr^{195} in TM5. The structural analyses illustrate the presence of intermolecular hydrogen bonds of AVC with residues Cys^{178}, Ser^{180}, Lys^{191}, and Thr^{195} of CCR5. *Panel B*, an intramolecular hydrogen bond network is seen involving Tyr^{37}, Glu^{283}, Met^{287}, and Tyr^{108}. Tyr^{37} is located in TM1, Tyr^{108} in TM3, and Glu^{283} and Met^{287} in TM7. Glu^{283} forms hydrogen bond interactions with the hydroxymethyl of AVC. Intramolecular hydrogen bonds are shown in *pink*, and the intermolecular hydrogen bonds in *green*. Note that the hydrogen bond networks spanning multiple domains should maintain the optimal shape of the cavity for the binding of AVC (Fig. 4, *A* and *B*). *Panel C*, the predicted van der Waals contact between AVC and CCR5 residues Lys^{191} and Ile^{198}. AVC is shown in *green spheres*, whereas Lys^{191} and Ile^{198} in *magenta*.

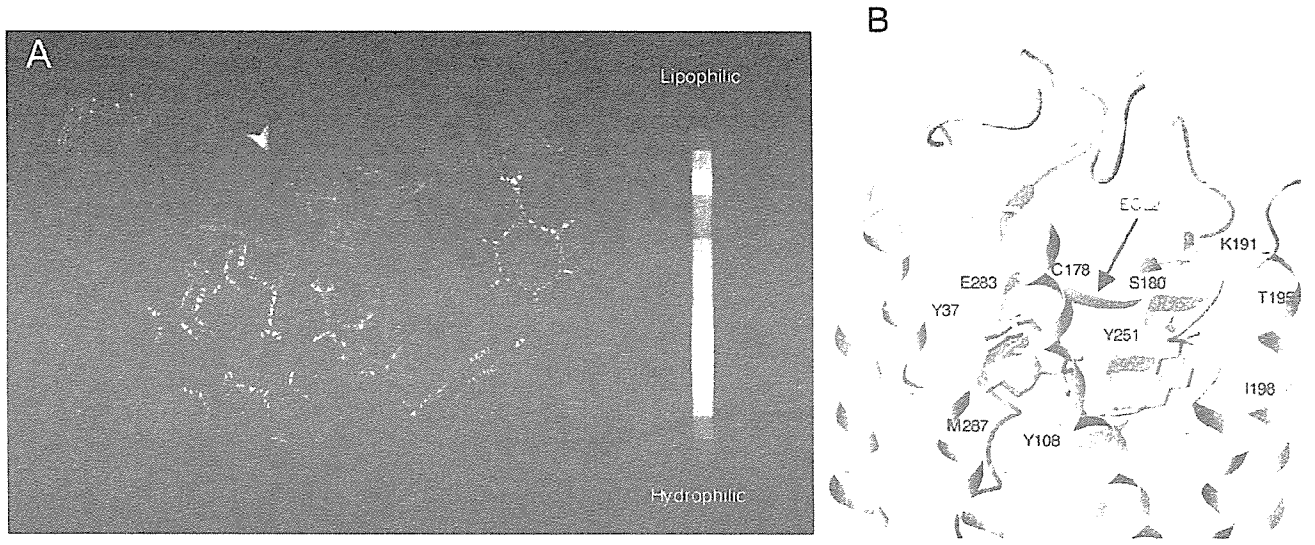

FIGURE 4. **The configuration of aplaviroc within CCR5.** *Panel A*, AVC lodged within the binding cavity of CCR5. The CCR5 cavity was defined with its lipophilic potential using MOLCAD. The region near the extracellular domain has some hydrophilic character (*red arrowhead*), whereas the rest of the cavity is mostly lipophilic. The carboxyl and hydroxymethyl of AVC interact with the hydrophilic regions of CCR5, whereas the rest of AVC interacts with the lipophilic regions of CCR5. *Panel B*, a docked structure of AVC (tube representation) bound to CCR5, illustrating the relative location of AVC within CCR5. Important binding site residues of CCR5 are shown in *wires*. Polar hydrogens are only shown. Note that TM1, 2, and 3 are toward the viewer from the plane and TM6 and 7 are away from the viewer behind the plane.

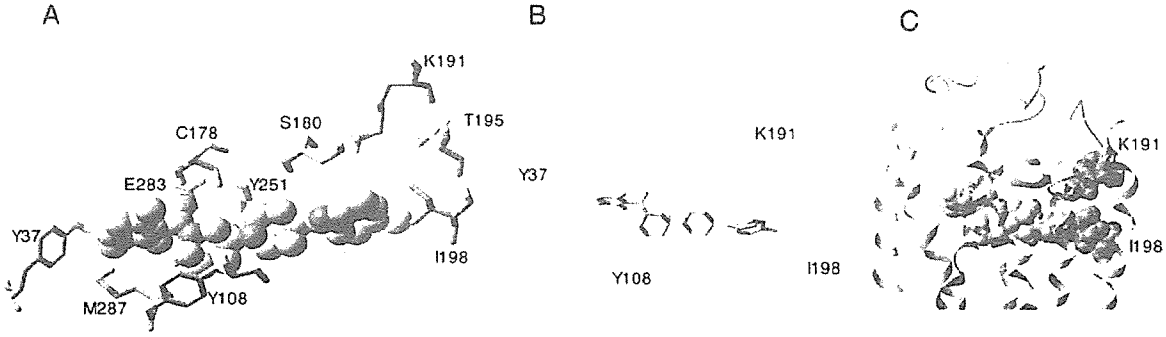

FIGURE 5. **Interactions of SCH-C with CCR5 residues.** *Panel A*, the configuration of SCH-C (shown in CPK) obtained with mutagenesis-based data (Table 1) combined with structural analyses. CCR5 residue orientations (shown in *tubes*) vary from that in Fig. 4 because conformational flexibility of receptors during docking of each inhibitor was taken into account. *Panel B*, Tyr^{37} forms hydrogen bonding interactions with SCH-C, and hence Y37A mutation reduces the binding affinity of SCH-C with CCR5. Note the location of Tyr^{108} and compare its corresponding location for the complex with TAK-779. SCH-C is shown in *tubes* and CCR5 residues in *wires*. Only polar hydrogens are shown in *panels A* and *B*. The molecules are colored by atom types (carbon, *gray*; oxygen, *red*; nitrogen, *blue*; hydrogen, *cyan*; sulfur, *yellow*; and bromine, *green*). *Panel C*, van der Waals interactions of SCH-C (*green*) with Lys^{191} and Ile^{198} (*magenta*). There is tight hydrophobic binding of SCH-C with Ile^{198}. Unlike AVC, Lys^{191} does not form significant interactions with SCH-C.

acts with the lipophilic region of CCR5 (Fig. 4, *A* and *B*). It is of note that AVC has a molecular weight of 614.2, larger than TAK-779 (M_r 531.1) and SCH-C (M_r 557.5), has a substantial hydrophobic contact and fits well inside the large binding cavity within CCR5 as shown in Fig. 4*A*. AVC also forms hydrogen bonds with Cys^{178}, Ser^{180}, Lys^{191}, and Thr^{195} (Fig. 3, *A* and *B*). It is presumed that these interactions with residues in multiple ECLs and the interface of extracellular and transmembrane domains are responsible for the tight binding of AVC to CCR5.

Amino Acid Substitutions Are Likely to Cause Substantial Conformational Changes in ECLs—Substitutions of amino acid residues, which are involved in hydrogen bonding, appear to directly and indirectly disrupt the hydrogen bond networks observed (Fig. 3, *A* and *B*). For example, Gly^{163}, located in TM4, does not interact directly with AVC, but is responsible for maintaining the shape of the binding cavity by its hydrogen bond interactions with Ser^{180} and Lys^{191} (Fig. 3*A*). Thus, the shape of the cavity is most likely altered with G163R substitution, and thereby AVC could lose critical interactions with ECL2 and TM5. In contrast, it was found that G163R exerts minimal effects on the binding of either SCH-C or TAK-779 to CCR5 (Table 1), potentially because these two inhibitors do not have direct hydrogen bond interactions with the ECL or ECL-TM interface.

As mentioned above, the carboxyl of AVC forms hydrogen bonds with Lys^{191} and Ser^{180} (Fig. 3*A*). The loss of binding with K191A substitution (Table 1) is likely because of the loss of the hydrogen bond with AVC as well as the altered shape of the cavity, which was confirmed by structural analysis of the $CCR5_{K191A}$-AVC complex. Neither SCH-C nor TAK-779 forms hydrogen bonds with Lys^{191} (Fig. 5, *A* and *B*, and Fig. 6*A*), hence it is thought that K191A substitution does not significantly affect the binding affinity of SCH-C or TAK-779 (Table 1). Ile^{198} located in TM5 has hydrophobic interactions with AVC (Fig. 3*C*). SCH-C and TAK-779 were predicted to have hydrogen bond interactions with Tyr^{37} located in TM1 (Fig. 5, *A* and *B*, and Fig. 6, *A* and *B*), whereas there appear to be no such interactions with AVC (Fig. 3*B*). This is consistent with the observation that Y37A substitution drastically changed the binding affinity of SCH-C and TAK-779 to CCR5 (Table 1). Ile^{198} forms a hydrophobic contact with SCH-C (Fig. 5*C*), although not much with TAK-779, which well explains the reason I198A reduces the K_D value of SCH-C with CCR5 but not that of TAK-

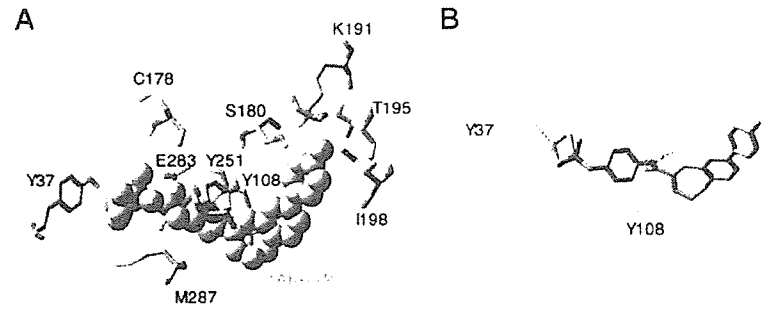

FIGURE 6. **Interactions of TAK-779 with CCR5 residues.** *Panel A*, the configuration of TAK-779 within the CCR5 binding pocket. *Panel B*, Tyr^{37} forms a hydrogen bonding interaction with TAK-779. Note the orientation of Tyr^{108} in comparison to the complex of CCR5 with SCH-C. Tyr^{108} forms π-π and hydrogen bond interactions with TAK-779 and represents a critical residue in agreement with the mutagenesis-based results (Table 1). Only polar hydrogens are shown. The molecules are colored by atom types (carbon, *gray*; oxygen, *red*; nitrogen, *blue*; hydrogen, *cyan*; sulfur, *yellow*).

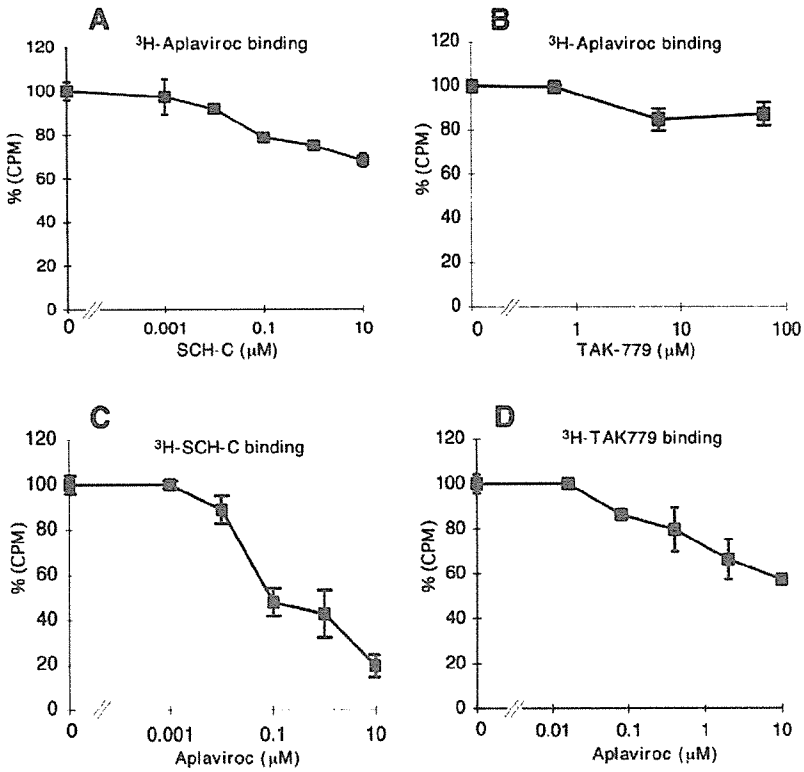

FIGURE 7. **Interactions between CCR5 inhibitors in relation to CCR5.** $CCR5_{WT}$-CHO cells were exposed to [^{3}H]AVC (3 nM; *panels A* and *B*), [^{3}H]SCH-C (3 nM; *panel C*), or [^{3}H]TAK-779 (10 nM; *panel D*), for 15 min, followed by the exposure to various concentrations (from 1 nM to 62.5 μM) of unlabeled SCH-C (*panel A*), TAK-779 (*panel B*), or AVC (*panels C* and *D*) for 30 min. The cells were then thoroughly washed, lysed, and the radioactivity of the lysates counted. All experiments were performed in duplicate and the data shown are mean values ± S.D. The amounts of the [^{3}H]CCR5 inhibitor bound to the cells are shown as mean % control values (each control value was obtained without an indicated unlabeled CCR5 inhibitor).

779 with CCR5 (Table 1). It is also of note that AVC has direct interactions with residues in the extracellular domain and its proximity (Cys^{178}, Ser^{180}, and Lys^{191}) (Fig. 3, *A* and *B*), which should strongly affect the conformation of extracellular loops in comparison to SCH-C and TAK-779, both of which failed to directly interact with the amino acid residues in the extracellular domain. The interaction of HIV-1-gp120 with ECLs is thought to be critical for the establishment of infection, therefore, one can assume that the binding of AVC to CCR5 should result in a significant loss of interactions with gp120, which could explain the significantly greater effect of AVC in blocking viral infectivity, compared with SCH-C and TAK-779. Thus, the data above suggest that the binding pockets are in the same general area within CCR5, however, the binding interactions of the three inhibitors with CCR5 residues substantially differ from each other, in particular between AVC and other two inhibitors.

Interactions between CCR5 Inhibitors in Relation to Their Binding to CCR5—All three CCR5 inhibitors examined in this study possess the properties of allosteric antagonists of CCR5, whereas AVC exerts only partial inhibition of the binding to CCR5 and physiological function of ^{125}I-RANTES in comparison to TAK-779 and SCH-C (11). Moreover, although the binding pocket for these inhibitors are all located in the same hydrophobic cavity within CCR5, their binding profiles substantially differ from each other as discussed above. Therefore, we analyzed the interactions of the three inhibitors in relation to $CCR5_{WT}$. When $CCR5_{WT}$-CHO cells were exposed to [^{3}H]AVC (3 nM) for 15 min, followed by the addition of various concentrations (1 nM to 10 μM) of unlabeled SCH-C, [^{3}H]AVC binding to CCR5 was reduced only moderately, by up to 32% (Fig. 7*A*). When the interaction between [^{3}H]AVC and unlabeled TAK-779 (0.625-62.5 μM) was examined, [^{3}H]AVC binding to CCR5 was not significantly replaced by unlabeled TAK-779 (Fig. 7*B*). On the contrary, when [^{3}H]SCH-C was added first and then unlabeled AVC was added, the binding of [^{3}H]SCH-C to $CCR5_{WT}$-CHO cells was significantly blocked (Fig. 7*C*). These data suggest that AVC effectively replaces [^{3}H]SCH-C and binds to $CCR5_{WT}$. The binding of [^{3}H]TAK-779 was likewise blocked by the addition of unlabeled AVC, although the extent of replacement by AVC was lesser as compared with the case of [^{3}H]SCH-C (Fig. 7*D*).

Role of Amino Acid Residues of CCR5 with Which Aplaviroc Is Associated in HIV-1 Infection and CC-chemokine Binding—In an attempt to define the biological and virological roles of amino acid residues, with which AVC is associated in this binding to CCR5, we selected 15 mutant CCR5-overexpressing CHO cells and examined profiles of sCD4/gp120

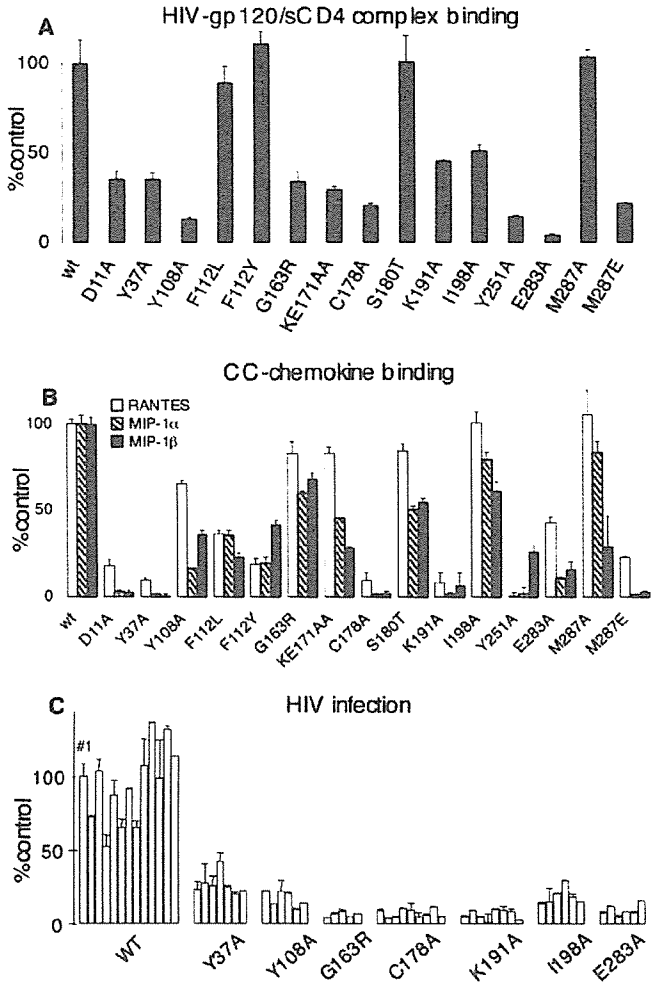

FIGURE 8. **Effects of amino acid substitutions in CCR5 on sCD4/gp120 binding, HIV infection, and CC-chemokine binding.** *Panel A*, profiles of the binding of sCD4/$gp120_{YU2}$ complex to various $CCR5_{MT}$ species overexpressing CHO cells. All values were normalized with the CCR5 expression level of each $CCR5_{MT}$ compared with that of $CCR5_{WT}$ (see "Experimental Procedures"). *Panel B*, profiles of the binding of ^{125}I-RANTES, ^{125}I-MIP-1α, and ^{125}I-MIP-1β to various $CCR5_{MT}$-expressing CHO cell preparations. All values were normalized with the CCR5 expression level of each $CCR5_{MT}$ compared with that of $CCR5_{WT}$. All assays were performed in duplicate or triplicate. *Panel C*, the susceptibility of various $CCR5_{MT}$-overexpressing U373-MAGI cells. For testing each $CCR5_{MT}$-overexpressing cell preparation, multiple clones were examined. In each set of experiments, $CCR5_{WT}$-clone 1 (*solid column*) served as a standard (100%).

binding and CC-chemokine (RANTES, MIP-1α, and MIP-1β) binding profiles. Nine of the 15 mutants were chosen based on the following reasons. Tyr^{108} was chosen because Tyr^{108} is within the aromatic cluster seen in the proximity of TM2 and TM3 and is reported to play a crucial role in the CC-chemokine-elicited activation of CCR5 (35). Y37A and E283A were chosen because Tyr^{37} and Glu^{283} are involved in the binding of the three inhibitors to CCR5 and have been shown to be highly conserved in CC-chemokine receptors including CCR5, CCR2B, CCR3, CCR1, and CCR4 (6). Six more mutants (G163R, C178A, K191A, I198A, Y251A, and M287E) were also chosen, with which the binding affinity of AVC was significantly reduced compared with $CCR5_{WT}$-expressing cells (>5-fold K_D difference) (Table 1). As shown in Fig. 8*A*, all 9 mutations described above decreased the sCD4/gp120 binding to CCR5 compared with that to $CCR5_{WT}$. It was noted that Y108A, Y251A, and E283A substitutions resulted in the greatest reduction of sCD4/gp120 binding.

We further determined the binding profiles of ^{125}I-RANTES, ^{125}I-MIP-1α, and ^{125}I-MIP-1β to the above 9 mutant CCR5-overexpressing CHO cell lines (Fig. 8*B*). In several CHO cell lines, the CC-chemokine binding profile notably differed from the HIV-gp120/sCD4 complex binding profile. Whereas both K191A and I198A substitutions caused moderate reduction in HIV-gp120/sCD4 complex binding (Fig. 8*A*), CC-chemokine binding was fairly preserved in $CCR5_{I198A}$-expressing cells, whereas CC-chemokine binding was almost completely reduced in $CCR5_{K191A}$-expressing cells. The G163R substitution preserved HIV-gp120/sCD4 complex binding by 34%, however, CC-chemokine binding was substantially spared by 68–83%.

We also employed six additional mutant CCR5-overexpressing CHO cells, which showed insignificant to minimal changes (less than 3-fold differences) in their K_D values compared with the K_D value for wild-type CCR5 (Table 1). Two substitutions in the extracellular domain of CCR5, D11A (NH_2 terminus) and KE171AA (ECL2), induced substantial reduction in HIV-gp120/sCD4 complex binding by 65 and 70%, respectively. The F112L, F112Y (both in TM3), S180T (ECL2), and M287A (TM7) substitutions caused no significant changes in K_D values (Table 1) or HIV-gp120/sCD4 complex binding (Fig. 8*A*). These data suggest that amino acid residues in the proximity of the hydrophobic cavity for AVC that do not change K_D values generally do not affect the HIV-gp120/sCD4 complex binding to CCR5. These 6 substitutions, however, caused CC-chemokine binding inhibition at various degrees, suggesting that the profile of the HIV-gp120/sCD4 complex binding to CCR5 differs from that of CC-chemokine binding to CCR5.

We finally generated seven clonal populations of $CD4^+$U373-MAGI cells expressing CCR5 with an amino acid substitution that caused significant reduction in the K_D values of either of the three CCR5 inhibitors and examined their susceptibility to HIV-1_{BaL} infection (Fig. 8*C*). HIV-1_{BaL} effectively infected $CCR5_{WT}$-expressing cells, however, the susceptibility to HIV-1_{BaL} infection was greatly reduced in $CCR5_{Y37A}$-, $CCR5_{Y108A}$-, and $CCR5_{I198A}$-expressing cells and that in $CCR5_{G163R}$-, $CCR5_{C178A}$-, $CCR5_{K191A}$-, and $CCR5_{E283A}$-expressing cells was more greatly limited. These data indicate that the mutations examined in this experiment effectively blocked HIV-1_{BaL} infection, although such mutations, in particular three mutations (G163R, K191A, and I198A), allowed some degree of sCD4/gp120 binding to $CCR5^+$ cells (Fig. 8*A*).

As noted above, the CC-chemokine binding profile notably differed from the profile of HIV-1_{BaL} infection susceptibility in $CCR5_{G163R}$- and $CCR5_{I198A}$-expressing cells. Moreover, moderate levels of chemokine binding were seen in $CCR5_{Y108A}$- and $CCR5_{E283A}$-expressing cells, whereas the least infection occurred in these cells. It should be of note that when we examined what ensued upon the binding of RANTES to $CCR5_{G163R}$-expressing cells, it was found that the level of Ca^{2+} flux that occurred in those cells was comparable with that in $CCR5_{WT}$-expressing cells following stimulation with RANTES.[3]

These data, taken together, suggest that the binding affinity of AVC seen with CCR5 variants generally paralleled the HIV-gp120/sCD4 complex binding affinity to mutant CCR5s, although it is of note that further fine-tuned analysis with greater numbers of CCR5 mutants is required for full understanding of the interactions among the HIV-gp120/sCD4 complex, CC-chemokines, and CCR5 inhibitors. The data also suggest that certain conformational changes caused by amino acid substitutions (*e.g.* at Tyr^{108}, Gly^{163}, or Ile^{198} residues of CCR5) might substantially reduce HIV-1 infection without significantly affecting physiological CC-chemokine-CCR5 interactions.

[3] K. Maeda, H. Nakata, T. Miyakawa, and H. Mitsuuya, unpublished data.

DISCUSSION

In the present study, we examined the structural and molecular interactions between CCR5 and three CCR5 inhibitors, AVC, SCH-C and TAK-779. When we exploited site-directed mutagenesis by generating a panel of mutant CCR5-expressing cells, and determined the K_D values of each CCR5 inhibitor with each mutant CCR5 species, the K_D values compiled corroborated our previous results obtained using the mAb replacement assay (11). We found that the binding affinity of AVC to wild-type CCR5 ($CCR5_{WT}$) was the greatest with a K_D value of 2.9 nM as compared with SCH-C and TAK-779 with K_D values of 16.0 and 30.2 nM, respectively (Table 1). It was also noted that the number of mutations that affected the binding of AVC was greater than in the cases of TAK-779 and SCH-C (Table 1). Moreover, the amino acid substitutions with which AVC turned out to have different K_D values were mostly located in the second extracellular loop (ECL2) and its interface with TM4 (Gly^{163}), or TM5 (Lys^{191}). By contrast, with regard to SCH-C and TAK-779, no substantially different K_D values were obtained with amino acid substitutions in ECL2 (Table 1). The data suggest that not only the binding interactions but also the molecular size and/or bulkiness of AVC are related to the different numbers of K_D-affecting mutations and different profile of K_D values obtained and that AVC forms substantial hydrophobic contacts with and fits well inside the hydrophobic cavity within CCR5 (Fig. 4*A*). It was also thought that such tight interactions of AVC with residues in ECLs and the interface of extracellular and transmembrane domains of CCR5 are responsible for the greater binding affinity of AVC to CCR5 as compared with two other inhibitors.

It was intriguing that certain amino acids such as Gly^{163} and Lys^{191} formed critical hydrogen bond networks in the interaction of AVC and CCR5 (Fig. 3, *A* and *B*). It was thought, therefore, that the amino acid substitutions in such positions dramatically altered the binding affinity of AVC to CCR5. It is also noteworthy that Cys^{178} of ECL2 is presumed to form a putative disulfide bridge with Cys^{101} of ECL1 and to be critical for the conformation of CCR5 (34). In the present study, C178A substitution, which should disrupt the putative disulfide bridge and cause significant conformational changes in both ECL1 and ECL2, nullified the CCR5 binding affinity of AVC, but not of SCH-C or TAK-779 (Table 1). In this respect, the lesser interactions of SCH-C and TAK-779 with extracellular domains (Table 1) are likely responsible for the lack of influence of the C178A substitution on the binding affinity of SCH-C and TAK-779, corroborating the notion that mutations in ECL2 did not alter the binding of SCH-C and TAK-779 to CCR5 (Table 1).

Two events are likely involved in the reduced binding of inhibitors to CCR5 with an amino acid substitution(s): (i) the alteration of direct interaction, if present, between the amino acid residue and the inhibitor and/or (ii) an allosteric effect(s) in which there is a significant conformational change(s) of CCR5 either near or distant from the mutated residue. In this respect, in the present work, we have shown that multiple hydrogen bond networks are important for the binding of AVC to CCR5 (Fig. 3, *A* and *B*). Some residues such as Lys^{191} directly interact with AVC, and hence mutations that lose this direct interaction are very likely responsible for the loss of binding. The lack of drastic changes in the binding of SCH-C and TAK-779, which are not predicted to directly interact with Lys^{191}, also supports this inference. Gly^{163}, however, does not directly bind to AVC but is a critical part of the Gly^{163}-Ser^{180}-Lys^{191}-Thr^{195} hydrogen network (Fig. 3*A*). Our molecular modeling, however, indicates that arginine at position 163 does not form hydrogen bonds with Ser^{180} or Lys^{191}. This alteration in the hydrogen bond network probably changes the shape of the cavity in the ECL2-TM4-TM5 region (an allosteric effect near the mutated residue) and results in reduced binding of AVC to $CCR5_{G163R}$. Mutation at residue 283 might be an example of the one causing an allosteric conformational change(s) distant from the mutated residue. Only AVC is predicted to directly interact with Glu^{283}, but a E283A mutation results in significant loss of binding for all three inhibitors examined. Thus, it is thought that certain amino acid substitutions reduce the binding of an inhibitor even though they are not directly interacting with the inhibitor. It is also of note that mutations at certain residues directly interacting with an inhibitor do not always cause significant loss of binding if CCR5 does not undergo a conformational change(s) or takes an alternate conformation that is not unfavorable for inhibitor binding.

Because a crystal structure of CCR5 is not available, unlike other targets for intervention of HIV infection including HIV reverse transcriptase (36), in the present study, in an attempt to conduct structural analyses of the interactions of CCR5 inhibitors with various mutant CCR5 species, an initial structural model of CCR5 was generated using homology modeling based on the crystal structure of bovine rhodopsin (23). The present approach of combining the site-directed mutagenesis-based data (Table 1) and molecular modeling should be a valuable strategy for gaining structural insights for membrane-bound proteins for which x-ray crystal structures are not as yet available. The CCR5-inhibitor complex structures were defined by iterative optimization of CCR5 and inhibitor structures. Mutated CCR5 structures were also defined and optimized based on the wild-type CCR5 structure, and minimized structures of various CCR5 mutants were used as starting structures for obtaining docked complexes of mutated CCR5 with inhibitors. It is of note that in the present study, our modeling study was combined and fine-tuned with the results of the saturation binding assay using a panel of mutant CCR5-expressing cells and tritiated CCR5 inhibitors and the resultant configuration and orientation of inhibitors docked within the hydrophobic cavity of CCR5 yielded a consistent analysis of the structure-activity data. The conformations of CCR5 without an inhibitor and CCR5 bound to an inhibitor are likely to be substantially different from each other because conformational changes are expected to occur upon inhibitor binding to CCR5. Thus, the conformational flexibility of both inhibitors and CCR species were taken into account in our analysis. In this regard, our ongoing analyses of binding affinity profiles using different ^{3}H-labeled CCR5 inhibitors and an expanded panel of mutant CCR5-expressing cell lines should further illuminate the intramolecular and intermolecular interactions of CCR5 and CCR5 inhibitors.

We also examined the binding profile of CCR5 inhibitors when one inhibitor was added to CCR5-overexpressing cells, followed by the addition of the second inhibitor (Fig. 7). Interestingly, when AVC first bound to CCR5 and SCH-C or TAK-779 was subsequently added, both SCH-C and TAK-779 only partially displaced AVC (Fig. 7, *A* and *B*). However, when SCH-C or TAK-779 first bound to CCR5 and AVC was subsequently added, SCH-C and TAK-779 were substantially displaced by AVC (Fig. 7, *C* and *D*). This ineffective displacement of AVC once bound to $CCR5_{WT}$ by SCH-C and TAK-779 could be explained by the difference of their K_D values (2.9 nM for AVC, 16 nM for SCH-C, and 30.2 nM for TAK-779 as illustrated in Table 1). However, it is of note that both SCH-C and TAK-779 failed to displace AVC even with very high concentrations: 3,333-fold (10 μM; Fig. 7*A*) and 20,833-fold (62.5 μM; Fig. 7*B*), respectively, greater than the [^{3}H]AVC concentration (3 nM). Thus, only the difference in K_D values among the three inhibitors unlikely fully explains the failure of AVC replacement by SCH-C and TAK-779. In this regard, a possible explanation is that AVC induces a series of significant conformational changes in CCR5 and, upon the completion of its stable lodging within the hydrophobic cavity within $CCR5_{WT}$, the binding and/or entry into CCR5 of the second inhibitor is